Biomaterials Science

ROYAL SOCIETY OF CHEMISTRY

PAPER

Published on 26 August 2026

Cite this: DOI: 10.1039/d6bm00877a

Customized pH-responsive poly(urethane)-based formulations treating chronic skin wound inflammation and promoting tissue regeneration

Rossella Laurano, *[a] Viviana Pinto Ribeiro,[b] Cláudia S. Oliveira,[b,c] Alessandro Torrisi,[a] Alessandro Ligas,[a] Monica Boffito, [a] Freni K. Tavaria,[b] Ana Leite Oliveira†[b] and Gianluca Ciardelli †[a]

Received 5th June 2026,
Accepted 25th August 2026

DOI: 10.1039/d6bm00877a

rsc.li/biomaterials-science

Severe inflammation and infections are major contributors to wound chronicity. Although various wound dressings have been engineered to deliver therapeutics locally, the lack of patient personalization is still a limiting factor. In this endeavor, this work aims to establish an adaptable therapeutic strategy by combining stimuli-responsive materials and 3D bioprinting for the prospective fabrication of shape-personalized patches capable of tuning payload release in response to the alkalinity of infected wound exudates. First, a –COOH-bearing amphiphilic poly(ether urethane) was synthesized and used to formulate thermo-/alkaline-pH-responsive hydrogels, while human recombinant lactoferrin (hrLF) was selected for its naturally derived therapeutic properties. Then, the hrLF-loaded hydrogel thermo-responsiveness was rheologically assessed, while the hrLF suitability for the biologically aggressive environment of chronic wounds was evaluated through UV/Vis spectroscopy and a colorimetric assay. Moreover, a finely tuned drug release was observed in response to pH *via* a non-Fickian diffusion mechanism. Furthermore, in *in vitro* studies on simplified inflamed wounds, hrLF promoted human dermal fibroblast proliferation (increased DNA content), exerted anti-inflammatory effects (reduced expression of TNF-α, IL-1β and IL-6), and exhibited bacteriostatic activity against *Staphylococcus aureus*. Finally, the hrLF-loaded hydrogel showed promising processability as a biomaterial ink. Overall, the engineered system showed strong adaptation to the dynamic wound environment.

Introduction

Upon skin injury, haemostasis and inflammation are the first stages of recovery. They play key roles in the normal wound healing process since the proper environmental conditions must be established for damaged tissue regeneration in a physiological time frame.[1] In more detail, haemostasis is responsible for platelet clot formation, and it is triggered by the extracellular matrix (ECM), which recruits platelets and provides information for their adhesion and aggregation.[2] Immediately after, the inflammation phase is governed by the activation of the immune cells, such as neutrophils and macrophages, through the secretion of reactive oxygen species (ROS), pro-inflammatory cytokines, proteases and growth factors to clean the wound bed by eliminating bacteria, pathogens and necrotic tissue and provide stimuli for regeneration.[3] Therefore, inflammation is an essential stage towards tissue healing. However, an excessive production of ROS and pro-inflammatory mediators leads to ECM damage and dysregulation of macrophage polarization towards the pro-inflammatory M1 or pro-regenerative M2 phenotype, ultimately creating a self-sustaining inflammation process.[1] As a consequence, the physiological inflammation phase turns into a pathological condition, making the wound stall in a chronic inflammation stage and thus leading to non-healing ulcers. To effectively manage chronic skin wounds, it is therefore crucial to control the progression of the inflammation phase and avoid its extension. In this scenario, the *in situ* delivery of anti-inflammatory agents is gaining increasing interest to locally reduce the persistent and excessive inflammation while avoiding systemic drug administration that could result in side effects on off-target tissues and organs. Besides traditional therapeutic agents, polyphenols,[4–6] terpenoids,[7–9] alkaloids,[10–12] and vitamins[13,14] have recently attracted wide research interest due to their natural origin and proven antioxidant and anti-inflam-

[a]*Department of Mechanical and Aerospace Engineering, Politecnico di Torino, Corso Duca degli Abruzzi 24, 10129 Turin, Italy. E-mail: rossella.laurano@polito.it*
[b]*Universidade Católica Portuguesa, CBQF–Centro de Biotecnologia e Química Fina–Laboratório Associado, Escola Superior de Biotecnologia, Rua Diogo Botelho 1327, 4169-005 Porto, Portugal*
[c]*RISE-Health, Faculty of Medicine, University of Porto, Alameda Prof. Hernâni Monteiro, 4200-319 Porto, Portugal*
† Co-last authorship.

matory properties. However, they are characterized by limited half-lives and stability in the characteristic harsh environment of chronic skin wounds.

A promising alternative is represented by lactoferrin, a native immunomodulatory protein secreted by neutrophils and known to recognize the immune activation of an organism and act as a first-line mediator in immune defence against pathogens and in the control of oxidative cell function.[15] Lactoferrin is a single 80 kDa polypeptide chain composed of 692 amino acids organized into two distinct lobes, each of them capable of sequestering ferric ions.[16] It is contained in most exocrine mammalian secretions (*e.g.*, saliva, tears, milk) and is known to be involved in the organism's host defence, being able to exert anti-inflammatory, antibacterial, antifungal, anti-tumor and anti-viral actions. Among the mentioned properties, the capability to work as a natural anti-inflammatory and anti-bacterial drug makes lactoferrin a promising therapeutic agent for the treatment of chronic wounds.[17] Regarding its anti-inflammatory activity, several different mechanisms have been identified: (i) inhibition of pro-inflammatory cytokine secretion (*e.g.*, IL-6, TNF-α) and augmented production of anti-inflammatory mediators (*e.g.*, IL-10);[16] (ii) reduction of ROS concentration due to iron scavenging activity,[18] and (iii) increased inhibition of neutrophil extracellular traps (NETs) through charge–charge interactions.[19] On the other hand, the antibacterial activity is known to be exerted through a double mechanism: iron-dependent as a consequence of lactoferrin affinity in binding or chelating iron,[20] and iron-independent, *i.e.*, attributed to the protein's capability to interact with the lipopolysaccharides (LPS) present in Gram-negative bacteria.[21]

Besides the selection of a proper therapeutic agent, great attention should also be paid to the selection of the most appropriate carrier for its delivery, since it should not only work as a vehicle but also play an active role in therapy administration to maximize its effectiveness. Indeed, the major critical issue characterizing currently available wound dressings is considered to be the uncontrolled payload release mechanism and kinetics. To overcome this limitation and move towards patient personalization, the exploitation of stimuli-responsive polymers for wound dressing engineering brings great advantages. For instance, engineering of biomaterials that are able to modify their physicochemical properties in response to a triggering stimulus from the wound microenvironment could enable smart control of drug delivery.[22,23] In this regard, the literature reports several examples of the design of smart formulations able to control payload release in response to temperature changes,[24,25] matrix metalloproteases (MMPs),[26,27] and ROS[28–30] concentrations and glucose levels.[31–33] Specifically, such stimuli have been successfully explored to engineer self-responding or externally triggered drug-releasing wound patches towards patient personalization.[34]

In this context, this work aims to exploit the characteristic alkalinity of infected wound exudate[35–37] by engineering an alkaline pH-sensitive hydrogel based on an in-house synthesized poly(ether urethane) (PEU) for the smart treatment of hard-to-heal wounds through the controlled release of lactoferrin. In detail, the successful optimization of the multi-stimuli-responsive PEU synthesis and functionalization, together with the capability of PEU hydrogels to respond to alkaline pH values, have been recently proven by comparing the release of a commercial low molecular weight drug (*i.e.*, ibuprofen) at pH 5 and 8.[38,39] Grounded on this knowledge, the present work intends to (i) investigate the capability of previously engineered hydrogels to adapt to the dynamic wound environment by finely tuning payload delivery within a wide pH range (*i.e.*, from 5 to 11) answering more precisely to patients' clinical needs; (ii) assess the protective action exerted by the vehicle towards the payload (*i.e.*, human recombinant lactoferrin, hrLF) under harsh conditions and (iii) study the anti-inflammatory and antibacterial properties of pH-released hrLF. Lastly, a proof-of-concept of the suitability of the system as a smart biomaterial ink has also been reported for the prospective fabrication of shape-personalized wound dressings.

Experimental

Materials

Poloxamer® 407 (P407), 1,6-hexamethylene diisocyanate (HDI), 1,4-cyclohexanedimethanol (CDM), dibutyltin dilaurate (DBTDL), human recombinant lactoferrin (hrLF, iron saturated), Toluidine Blue O (TBO), phosphate buffered saline (PBS) tablets, lithium bromide (LiBr), QuantiPro™ bicinchoninic acid (BCA) assay, Dulbecco's modified Eagle's medium (DMEM), monobasic potassium phosphate (KH_2PO_4), sodium phosphate dibasic dihydrate ($NaHPO_4{\cdot}2H_2O$), hydrochloric acid (HCl), sodium hydroxide (NaOH) and lipopolysaccharide from *Escherichia coli* (O111:B4) (LPS) were purchased from Merck Life Science (Italy). CellTiter-Blue® Cell viability assay and CytoTox-ONE™ Homogeneous Membrane Integrity Assay were received from Promega (Italy), while the live and dead assay, Human Lactoferrin ELISA kit and TRIzol reagent were obtained from Life Technologies (Italy). Propidium iodide was purchased from Biolegend (Portugal) and RNAse from Thermo Fisher Scientific (USA). Calf bovine serum (BCS), foetal bovine serum (FBS) and NIH-3T3 murine fibroblasts (CRL-1658) were purchased from ATCC® (Italy). Mycozap PLUS and MycoAlert PLUS mycoplasma detection kits were received from Lonza (The Netherlands). Direct-zol™ RNA MiniPrep kit was obtained from Zymo Research (USA), while qScript cDNA Synthesis kit and PerfeCta SYBR Green FastMix kit were purchased from Quanta Biosciences (USA). 1,2-Dichloroethane (DCE), anhydrous methanol, diethyl ether (DEE), petroleum ether, chloroform and *N*,*N*-dimethylformamide (DMF) were purchased from Carlo Erba Reagents in analytical grade and used as received if not further specified.

P-CHP407 synthesis and powder plasma treatment

The synthesis and functionalization of the thermo- and alkaline pH-responsive poly(ether urethane) with the acronym P-CHP407 were performed according to recently optimized procedures.[38] Briefly, P407, HDI, DCE and CDM were first

treated to remove residual water molecules;[40] then, a two-step reaction synthesis was carried out by reacting the P407 macrodiol (20% w/v in anhydrous DCE) and HDI in 1 : 2 molar ratio at 80 °C for 150 minutes in the presence of catalytic amounts of DBTDL (0.1% wt/wt with respect to the macrodiol). The obtained low molecular weight isocyanate-terminated poly(ether urethane) was then chain-extended at 60 °C for 90 minutes upon the addition of CDM at a 1 : 1 molar ratio. Finally, the reaction was stopped through the addition of anhydrous methanol, and the polymer (CHP407) was collected through precipitation in petroleum ether (4 : 1 v/v with respect to the DCE total volume). Subsequently, CHP407 was dissolved at 20% w/v in DCE, purified through precipitation in DEE/methanol (98/2 v/v, 5 : 1 v/v with respect to DCE) and collected by centrifugation before allowing it to dry in a fume hood.

Afterwards, 5 g of CHP407 powder with controlled diameter (*i.e.*, <500 μm) was plasma-treated in the presence of acrylic acid vapor to expose carboxylic acid groups by using a plasma reactor equipped with a rotary system (Diener Electronic, Germany). Specifically, the functionalization was carried out according to a two-step procedure: (i) surface activation through the application of a direct power supply at 50 W for 5 minutes under argon flow at 10 sccm, followed by (ii) reactor filling with acrylic acid (10 μL min^{-1} for 15 minutes) and grafting/polymerization through the activation of the generator in an alternated mode at 200 W (9 Hz, Pulse ON 10 ms, Pulse OFF 1000 ms, Duty Cycle 0.01, mean power applied 22 W) for 10 minutes. The functionalized polymer, referred to as P-CHP407, was dissolved in chloroform at 2.5% w/v, precipitated in petroleum ether at 5 : 1 v/v to remove unreacted acrylic acid, dried in a fume hood, and stored under vacuum until use.

P-CHP407 chemical characterization

Attenuated Total Reflectance Fourier Transform Infrared (ATR-FTIR) spectroscopy and Size Exclusion Chromatography (SEC) analyses were conducted on P407, CHP407 and P-CHP407 according to a previously published work.[41] Briefly, the ATR-FTIR characterization was performed by using a PerkinElmer Spectrum 100 (PerkinElmer Inc., USA) equipped with an ATR accessory (UATRS KRSS, PerkinElmer, USA) with a diamond crystal. Spectra were recorded using 32 scans in the range 4000–600 cm^{-1} with a resolution of 4 cm^{-1}.

An Agilent Technologies 1200 Series (Agilent Technologies Inc., USA) equipped with a Refractive Index (RI) detector and two Water Styragel columns (HR1 and HR4) kept at 55 °C was used for SEC analyses. Polymers were first dissolved in the mobile phase (*i.e.*, DMF added with 0.1% w/v LiBr) at 2 mg mL^{-1}, and then filtered through a 0.45 μm syringe filter (poly (tetrafluoroethylene) membrane, Whatman). Poly(ethylene glycol) standards with peak molecular weight in the range 4–200 kDa were used to estimate the number average molecular weight ($\bar{M}_n$), weight average molecular weight ($\bar{M}_w$) and polydispersity index (D) of the analyzed polymers.

Moreover, TBO colorimetric assay was performed on CHP407 and P-CHP407 samples to quantify the number of exposed –COOH groups.[38] Briefly, polymers were first dissolved at 0.05% w/v in the dye solution (500 μM) adjusted to pH 10 and then incubated for 18 h in the dark to allow electrostatic bonding between the –COOH groups and dye molecules. Subsequently, samples were dialyzed for 7 days (3.5 kDa cut-off membrane) against double-distilled water (ddH_2O) and lyophilized. Lastly, 10 mg of freeze-dried samples were dissolved in 1 mL of acetic acid/ddH_2O (50/50 v/v) for 30 minutes at room temperature (RT) in the dark, and the extract absorbance was measured at 632 nm using a UV/Vis spectrophotometer (Lambda 25, PerkinElmer, USA). The absorbance of the standard solutions, prepared by dissolving the TBO powder in acetic acid/ddH_2O (1–50 μM), was measured and used as a calibration curve for the quantification of –COOH groups. Analyses were performed in triplicate, and the results are reported as mean ± standard deviation.

Hydrogel formulation

P-CHP407 gelling formulations were prepared by dissolving the polymer at 15% w/v concentration in physiological saline solution (0.9% NaCl).[38] Differently, P-CHP407 hydrogels loaded with hrLF (*i.e.*, P-CHP407_hrLF) were prepared by first dissolving the protein in physiological saline solution at 2 mg mL^{-1}, then using this solution as a solvent for P-CHP407 dissolution. For both formulations, systems were kept at 4 °C overnight to allow complete dissolution before being further tested.

Rheological characterization

The thermo-responsiveness of the hrLF-loaded and unloaded hydrogels was rheologically evaluated using a stress-controlled rheometer (MCR302, Anton Paar GmbH, Austria) equipped with a 25 mm parallel plate geometry and a Peltier system for temperature control. First, the linear viscoelastic (LVE) region was identified by studying the gel response to applied deformation through strain sweep tests at 37 °C (10 Hz, strain range 0.01%–500%). Then, temperature ramp tests in continuous (deformation rate 0.1 s^{-1}) and oscillatory (10 Hz, 0.1% strain) conditions were conducted in the range 0 °C–40 °C, at 2 °C min^{-1} temperature increase. Lastly, the viscoelastic properties were analyzed through frequency sweep tests within the LVE region at 37 °C (0.1% strain, frequency range: 0.1–100 rad s^{-1}). Formulations were prepared as previously described, and analyses were conducted by setting a 0.4 mm gap between the plates. Before each test, samples were poured on the lower plate of the rheometer in the sol state, heated at the test temperature, and equilibrated for 10 minutes.

Human recombinant lactoferrin stability in buffers

The stability of hrLF in contact with buffers at different pH values was directly and indirectly assessed through UV/Vis spectroscopy and the BCA colorimetric assay, respectively. For this purpose, $Na_2HPO_4{\cdot}2H_2O$, KH_2PO_4, HCl and NaOH were first dissolved in ddH_2O at 0.1 M salt concentration; then, buffers with pH values between 5 and 11 were obtained by mixing the stock solutions according to the volumes listed in Table 1.

Table 1 Volumes of the acid and base solutions required for the preparation of the buffers at pH 5, 7, 9 and 11. Stock solutions were obtained by dissolving the salts in ddH_2O at 0.1 M concentration

Buffer pH	$Na_2.HPO_4{\cdot}2H_2O$ (mL)	KH_2PO_4 (mL)	HCl (mL)	NaOH (mL)
5	0.25	9.75	—	—
7	6.90	—	3.10	—
9	9.24	—	0.40	0.36
11	8.50	—	—	1.50

Subsequently, hrLF standards were prepared by dissolving the protein in each buffer at concentrations in the range 0.1–0.4 mg mL^{-1} and 1–30 μg mL^{-1}, and analyzed through UV/Vis spectroscopy and BCA assay, respectively, after 0 h, 24 h, 48 h, 72 h, 96 h and 7 d of incubation at 37 °C. Specifically, UV/Vis analyses were performed by measuring the peak absorbance at 280 nm (corresponding to the hrLF aromatic rings) using a UV/Vis spectrophotometer (Lambda 25, PerkinElmer, USA), while the BCA assay was conducted following the manufacturer's instructions. Briefly, the BCA working solution was first prepared by mixing reagents QA, QB and QC at a 25 : 25 : 1 ratio; then, 150 μL of this solution was added to the same volume of hrLF samples and incubated at 60 °C for 1 h to allow Cu^{2+} ion reduction. Lastly, the absorbance at 560 nm was measured using a Victor X3 plate reader (PerkinElmer, USA).

Human recombinant lactoferrin release test against buffers

In vitro pH-controlled hrLF release tests were conducted by incubating P-CHP407_hrLF hydrogels in contact with buffers at pH values ranging between 5 and 11. For this purpose, protein-loaded systems (1 mL) were prepared as previously described, incubated at 37 °C for 15 minutes to ensure a complete sol-to-gel transition, and then put in contact with 1 mL of buffer prepared as reported in Table 1 and equilibrated at the test temperature. hrLF unloaded systems (*i.e.*, P-CHP407 hydrogels) were also tested as a control. Afterwards, extracts were collected at 30 min, 60 min, 90 min, 2 h, 4 h, 6 h, 24 h, 30 h, 48 h, 54 h, 72 h and 7 d of incubation and analyzed with the BCA colorimetric assay. For each considered pH condition, the released amounts of hrLF were quantified by referring to calibration curves prepared by dissolving the protein in the corresponding pH buffer at concentrations within the 1–30 μg mL^{-1} range and analyzed according to the same procedure. Analyses were performed in quintuplicate, and the percentages of released hrLF were expressed as mean values ± standard deviation. Lastly, the Korsmeyer-Peppas model was implemented as reported by Laurano and Torchio *et al.*[42] to define the transport mechanism based on the estimated release exponent n value.

Enzyme-linked immunosorbent assay

To assess the preservation of hrLF native conformation upon release from P-CHP407 hydrogels in contact with buffers at different pH values, extracts from drug-release tests were also analyzed through the ELISA assay according to the manufacturer's instructions. Briefly, antigen binding was performed by adding 100 μL of sample to each of the 96 wells and by incubating the multiwell plate for 2.5 h at RT. Subsequently, biotin binding to the antigen was carried out by adding 100 μL of biotin conjugate and incubating for 1 h at RT. Then, biotin–streptavidin binding was induced by adding 100 μL of streptavidin-HRP solution to each well and waiting 45 minutes at RT. Lastly, 100 μL of tetramethylbenzidine (TMB) substrate was added to each well and the plate was incubated for 30 minutes at RT, in the dark, under gentle stirring to allow TMB conversion into a blue-colored product. Finally, the absorbance was measured at 450 nm by using a multimode plate reader (Victor X3, PerkinElmer, USA). Analyses were performed in triplicate, and the results are reported as mean values ± standard deviation.

In vitro cytocompatibility of hydrogel extracts

Hydrogel cytocompatibility was indirectly tested through extract contact with murine fibroblasts for 24 h according to the ISO 10993-5 regulations. For this purpose, P-CHP407 and P-CHP407_hrLF formulations were prepared as previously described and put in contact with complete culture medium (*i.e.*, DMEM supplemented with Mycozap PLUS and 10% v/v BCS) for 24 h (1 mL of medium *vs.* 100 mg of samples). NIH-3T3 murine fibroblasts were first seeded in a 96-well plate at 7500 cells per well and allowed to grow for 24 h in a humidified incubator at 37 °C, 5% CO_2 to achieve confluence. Then, the medium was replaced with 100 μL of extract and the plate was incubated in normal culture conditions for 24 h. Cells cultured in complete medium and treated with a lysing solution were used as negative and positive cytotoxicity controls, respectively. Lastly, cell metabolic activity and cytotoxicity were assessed through the CellTiter-Blue® and CytoTox-ONE™ assays according to the manufacturer's instructions as previously described.[43] Fluorescence was then measured at E_x/E_m 530/590 nm through a multi-mode plate reader Victor X3 (PerkinElmer, USA), and the results are expressed as percentages with respect to the controls. Analyses were performed in quintuplicate, and the results are reported as the average values ± standard deviation of three independent assays. Before each assay, cells were tested for mycoplasma contamination by using the MycoAlert PLUS mycoplasma detection kit.

Furthermore, to visually assess cell viability, the live and dead assay was also performed on extract-treated NIH-3T3 murine fibroblasts. To this purpose, cells were first seeded and treated as previously described; then, upon extract removal, they were washed with PBS and added with calcein AM and ethidium homodimer-1 at 2 μM and 4 μM concentration, respectively. Subsequently, the plate was incubated at RT for 20 minutes, and, lastly, cells were imaged under an inverted microscope (Leica Microsystems, Germany).

In vitro cytocompatibility of released human recombinant lactoferrin

The cytocompatibility of hrLF at concentrations mimicking the amounts of protein released as a function of pH and time was

tested on human dermal fibroblasts (HDFs) regularly cultured in DMEM supplemented with 10% v/v FBS and 1% v/v Pen/Strep and grown in a humidified incubator at 37 °C and 5% CO_2. When at confluence, cells were enzymatically detached by adding TrypLE™ and used for the following assays.

Metabolic activity of hrLF-treated human dermal fibroblasts. The influence of hrLF on HDF metabolic activity was investigated through the Alamar Blue assay. To this purpose, hrLF was dissolved in complete culture medium at concentrations ranging from 10 to 500 μg mL^{-1} and sterile-filtered through 0.22 μm filters. HDFs were seeded in a 48-well plate at a density of 20×10^3 cells per well and cultured in normal conditions to allow adherence. After 24 h, the medium was removed, replaced with 600 μL of hrLF solutions, and the plates were incubated again at 37 °C, 5% CO_2 for 24 h, 48 h and 5 d. Cells cultured in complete medium and treated with latex rubber residues were used as negative and positive cytotoxicity controls, respectively. At each time point, 400 μL of Alamar Blue solution (10% v/v in complete medium) was added to each well upon medium removal, and the plate was incubated at 37 °C, 5% CO_2 in the dark for 3 h. Lastly, fluorescence was measured at E_x/E_m 550/605 nm using a microplate reader (Synergy HT, BioTek Instruments, USA), and the metabolic activity was expressed as a percentage with respect to the negative control. The analyses were performed in triplicate, and the results are reported as average values ± standard deviation of three independent assays.

Cell cycle assay on hrLF-treated human dermal fibroblasts. Cell cycle assays were conducted to study the influence of hrLF at the highest tested concentration (*i.e.*, 500 μg mL^{-1}) on HDFs. For this purpose, cells were seeded in a 6-well plate at 50×10^3 cells per well and incubated under normal culture conditions for 48 h. Afterwards, the medium was replaced with 2 mL of hrLF solution and the plate was incubated again for 24 h, 48 h and 5 d. Cells cultured in complete DMEM were used as the negative control. Cells were not synchronized before treatment. At each time point, cells were carefully collected, cooled in an ice bath for 15 minutes, and then fixed by adding 1.5 mL of ice-cold 96% ethanol. Before the analysis, cells were washed twice with PBS and collected by centrifugation (125 rpm, 5 minutes). Then, 50 μL of RNase A solution (200 μg mL^{-1} in 1% w/v sodium citrate) was added to each Eppendorf and incubated at 37 °C for 15 minutes. Lastly, 50 μL of a propidium iodide staining solution (0.5 mg mL^{-1} in 1% w/v sodium citrate) was added, and the cells were kept at RT in the dark for 30 minutes before being analyzed with a flow cytometer (BD Accuri C6 Plus, USA). Approximately 10 000 events were acquired for each sample. Gating strategies were carefully adjusted to exclude debris and non-cellular events. Gate settings were established and validated using PBS-only controls and unstained cell controls to ensure accurate identification of the cell population of interest.

The analyses were performed in triplicate, and results are reported as average values ± standard deviation of three independent assays.

Human recombinant lactoferrin features in inflamed wound mimicking conditions

To study the biological activity exhibited by hrLF in a wound-mimicking environment, HDFs were first treated with LPS to induce inflammation according to the protocol reported by Feldo *et al.*[44] For this purpose, HDFs were seeded at 10×10^3 cells per well in a 96-well plate and grown under normal culture conditions for 24 h. Then, the medium was replaced with 150 μL of LPS solution (10 μg mL^{-1} in complete medium) and the plate was incubated again in a humidified incubator at 37 °C, 5% CO_2. Cells cultured in complete medium and treated with latex rubber residues were used as negative and positive controls, respectively. After 24 h, LPS was removed, and the cells were treated with 200 μL of hrLF at 100 μg mL^{-1}, 500 μg mL^{-1} and 750 μg mL^{-1} for 24 h, 48 h and 5 d. Lastly, the metabolic activity of HDFs and their capability to reduce inflammation and promote tissue regeneration were studied using the Alamar Blue Assay, RT-PCR and DNA quantification, respectively.

Alamar Blue assay. The metabolic activity of HDFs treated with hrLF upon the induction of an inflammation state was investigated using the Alamar Blue assay performed after 24 h, 48 h and 5 d of incubation. The assay was performed according to the previously described procedure, and the results are reported as average values ± standard deviation of three independent experiments.

DNA quantification. The DNA concentration of untreated- and hrLF-treated HDFs cultured in inflamed wound-mimicking conditions was quantified using a Thermo Scientific™ Multiskan™ GO Microplate Spectrophotometer (Thermo Fisher, USA). For this purpose, at each time point, 100 μL of ultrapure water was first added to each well; then, the cells were mechanically detached, and, lastly, DNA isolation was carried out by inducing thermal shock. Specifically, collected cells were first kept at 37 °C for 1 h and then stored at −80 °C for at least 24 h. Lastly, 2 μL of each sample was analyzed by measuring the absorbance at 260 nm. Analyses were performed in triplicate, and the results are reported as average values ± standard deviation of three independent assays.

Quantification of pro- and anti-inflammatory markers through RT-PCR. The expression of pro- and anti-inflammatory markers in HDFs treated with hrLF upon the induction of an inflammation state was investigated using RT-PCR analyses. For this purpose, at each time point, cells were mechanically detached, mixed with 100 μL of TRIzol to ensure complete lysis and RNase activity inhibition, and stored at −80 °C until use. Subsequently, RNA extraction was performed by using the Direct-zol™ RNA MiniPrep kit according to the manufacturer's instructions, followed by total concentration and purity determination by measuring the absorbance at 260 nm using a NanoDrop Lite Plus spectrophotometer (Thermo Fisher, USA) and by calculating the A_{260}/A_{280} absorbance ratio, respectively. Only samples with A_{260}/A_{280} ratios ranging between 1.6 and 2.0 were considered for first-strand complementary DNA (cDNA) synthesis, performed using a qScript cDNA Synthesis kit

Table 2 List of the primers and their corresponding melting temperatures (T_m)

Gene name	Gene symbol	NCBI	Primer forward	Primer reverse	T_m (°C)
Glyceraldheyde-3-phosphate dehydrogenase	GADPH	NM_002046.7	ACAGTCAGCCGCATCTTCTT	GACAAGCTTCCCGTTCTCAG	52
Tumor necrosis factor	TNF-α	NM_000594.3	TGAGGCCAAGCCCTGGTATGAG	CCCAGACTCGGCAAAGTCGAGA	58
Interleukin-6	IL-6	NM_000600.4	AGCCAGAGCTGTGCAGATGAGT	CTTCGTCAGCAGGCTGGCATTT	58
Interleukin-1β	IL-1β	NM_000576.3	AGAAGTTACCTGAGCTCGCCA	AGTGGTGGTCGGAGATTCGT	52
Interleukin-10	IL-10	NM_001382624.1	CCTCCGCCAATCTCTCACTCA	GTTCTCCCCCAGGGAGTTCAC	58
Collagen type III	COL III	NM_000090.4	ACACGCAAGGCTGTGAGACT	TGTCGGTCACTTGCACTGGT	52

according to the supplier's instructions. Afterwards, the synthesized cDNA was used for the amplification of the genes reported in Table 2 using the PerfeCta SYBR Green FastMix kit, following the provided protocol. A total of 45 cycles dealing with denaturation (95 °C, 5 s), annealing (specific temperature for each gene, 15 s), and extension (72 °C, 10 s) were performed using a CFX Connected Real-Time PCR Detection System (Bio-Rad, USA). GADPH was considered as a reference gene for data normalization to compensate for variations in the quantities of cDNA used as a template. The quantity of target nucleic acids in equivalent amounts of different samples was compared through relative quantification. Specifically, the expression levels of cells treated with LPS-conditioned medium at each time point were used as calibrators.

Subsequently, the Livak ($2^{-\Delta\Delta C_T}$) method was adopted to calculate the expression level of each target gene with respect to the calibrator upon the measurement of the threshold cycle (C_T) values. C_T values of the tested samples and calibrator were normalized considering the reference gene (ref.), and, lastly, the ΔC_T of each sample was obtained according to the following formula:

$$\Delta\Delta C_T = \frac{C_{T(\text{target, test})} - C_{T(\text{ref., test})}}{C_{T(\text{target, calibrator})} - C_{T(\text{ref., calibrator})}}.$$

Analyses were performed in duplicate, and the results are reported as average values ± standard deviation of three independent experiments.

In vitro antimicrobial properties of human recombinant lactoferrin

The antibacterial activity of hrLF was evaluated against Gram-positive *Staphylococcus aureus* (ATCC6538) and Gram-negative *Escherichia coli* (ATCC8739). For this purpose, bacteria from single colonies were first incubated in Mueller-Hinton Broth (MHB, Biokar Diagnostics) at 37 °C overnight. The resulting cultures were then diluted to achieve a final concentration of 10^8 colony-forming units (CFU) per mL. Subsequently, hrLF was dissolved at a stock concentration of 10 mg mL^{-1} in MHB and diluted at 1 : 10 to obtain an intermediate solution. Antibacterial assays were performed in 96-well plates by mixing 50 μL of hrLF solution with 50 μL of bacterial suspension, resulting in a final hrLF concentration of 500 μg mL^{-1}. Control samples were composed of bacterial suspension prepared under identical conditions but without hrLF. The plate was incubated at 37 °C for 24 h. Following incubation, bacterial viability was assessed by colony counting. Briefly, 50 μL aliquots from each well were serially diluted in Ringer's solution (Biokar Diagnostics) by transferring 50 μL of sample into 450 μL of diluent, generating dilutions up to 10^{-8}. Subsequently, 20 μL of each dilution was plated on Mueller-Hinton agar (Biokar Diagnostics) plates and incubated at 37 °C for an additional 24 h. Lastly, the number of bacterial colonies was recorded after 6 h and 24 h of incubation, and CFU counts were used to determine the potential antibacterial activity of hrLF. The results are reported as average values ± standard deviation of three independent assays.

Proof of concept of printability

To study hydrogel processability as biomaterial ink, two different logos were first designed by using Rhinoceros 6.0 CAD software, and then extruded by using the Inkredible + CellInk bioprinter (CellInk, Sweden) equipped with a pneumatic syringe for ink extrusion. An open-source slicing software (*i.e.*, Slic3r) was used to convert the 3D virtual model into the corresponding g.code. For this purpose, P-CHP407_hrLF hydrogels were prepared, loaded into the appropriate cartridge, and equilibrated at the extruding temperature (*i.e.*, 22 °C) for 10 minutes to allow the achievement of a semi-gel state. Subsequently, the ink was extruded through a 25G conical nozzle by setting 37 °C, 150 kPa and 7.5 mm min^{-1} as bed temperature, extrusion pressure and printing speed, respectively. The printed logos were then imaged and compared to the corresponding virtual model.

Statistical analysis

Statistical analysis was performed using GraphPad Prism 8.0 for Windows 10 (GraphPad Software, La Jolla, USA; https://www.graphpad.com). Two-way ANOVA analysis followed by Šídák's multiple comparisons test was used to compare results, and the statistical significance of each comparison was assessed as follows: $p < 0.0001$ extremely significant (****); $0.0001 < p < 0.001$ extremely significant (***); $0.001 < p < 0.01$ very significant (**); $0.01 < p < 0.05$ significant (*) and $p \geq 0.05$ not significant (ns).

Results and discussion

P-CHP407 chemical properties

An in-depth characterization of the physicochemical properties of the P-CHP407 polymer was presented in our previously published papers focused on the optimization of the synthesis

and functionalization protocols leading to the design of a high molecular weight poly(ether urethane) responsive to temperature and alkaline pH.[38,40] Thus, in this work, results from ATR-FTIR spectroscopy (Fig. S1), SEC analyses (Table S1) and TBO colorimetric assay (Fig. S2) were reported in the SI as proof of the success of both the synthesis and the plasma treatment. Specifically, the comparison of ATR-FTIR spectra recorded for P407 macrodiol and unfunctionalized CHP407 polymers first confirmed the successful synthesis of a poly (ether urethane) through the appearance of characteristic vibrational bands ascribed to urethane bonds; moreover, the complete overlap of CHP407 and P-CHP407 spectra also demonstrated the absence of functionalization-induced degradation phenomena. Such qualitative results were further supported by chromatographic analyses, which showed higher $\bar{M}_n$ and $\bar{M}_w$ values for CHP407 and P-CHP407 samples than for P407. In addition, the absence of difference between the $\bar{M}_n$ and D values of CHP407 and P-CHP407 further corroborated the preservation of polymer chain integrity upon plasma treatment. Lastly, the colorimetric quantification of –COOH groups confirmed the grafting/exposure of $4.7 \times 10^{18} \pm 5.6 \times 10^{17}$ units per g of polymer.

Thermo-responsiveness of hrLF-loaded smart hydrogels

The capability of drug-loaded PEU hydrogels to preserve their temperature-induced gelation mechanism has already been investigated as a function of the wettability and concentration of the encapsulated drug molecules.[45] Specifically, low molecular weight molecules (*i.e.*, approx. 200 Da) were selected for that purpose. Differently, the influence of the encapsulation of a high molecular weight protein on a temperature-guided polymeric chain arrangement has not been studied before. Therefore, continuous and dynamic temperature ramp tests were first performed on P-CHP407 and P-CHP407_hrLF formulations to study whether hrLF encapsulation affected the gelation kinetics (Fig. 1B and C).

As illustrated in Fig. 1A, both unloaded and hrLF-loaded formulations were able to undergo gelation within a few minutes upon temperature increase. Rheologically, P-CHP407 and P-CHP407_hrLF systems showed very similar viscosity profiles (Fig. 1B) characterized by three main intervals: (i) an initial viscosity decrease as a function of temperature increase for all the fluids; (ii) a sharp viscosity increase due to micelle nucleation, growth and progressive packing and (iii) a sudden viscosity decrease ascribed to micelle disentanglements. In more detail, the comparison between unloaded and hrLF-loaded systems did not evidence significant differences in the initial viscosity values (*i.e.*, 0.66 *vs.* 0.62 Pa s^{-1}) or the temperature at the minimum viscosity value (*i.e.*, T_{onset} – 16.7 °C *vs.* 17 °C), meaning that protein addition to the system did not alter the mechanism or kinetics of the temperature-driven polymeric chain arrangement into micelles. Conversely, slightly different temperatures (*i.e.*, 34 °C and 35.4 °C for P-CHP407_hrLF and P-CHP407, respectively) marked the beginning of the third phase, thus suggesting the establishment of a more developed but weaker gel network in the presence of lactoferrin.

The dynamic temperature ramp test (Fig. 1C) further confirmed the preservation of P-CHP407_hrLF hydrogel thermo-responsiveness, giving sol–gel transition temperatures equal to 28.0 °C and 28.2 °C for hrLF-loaded and unloaded formu-

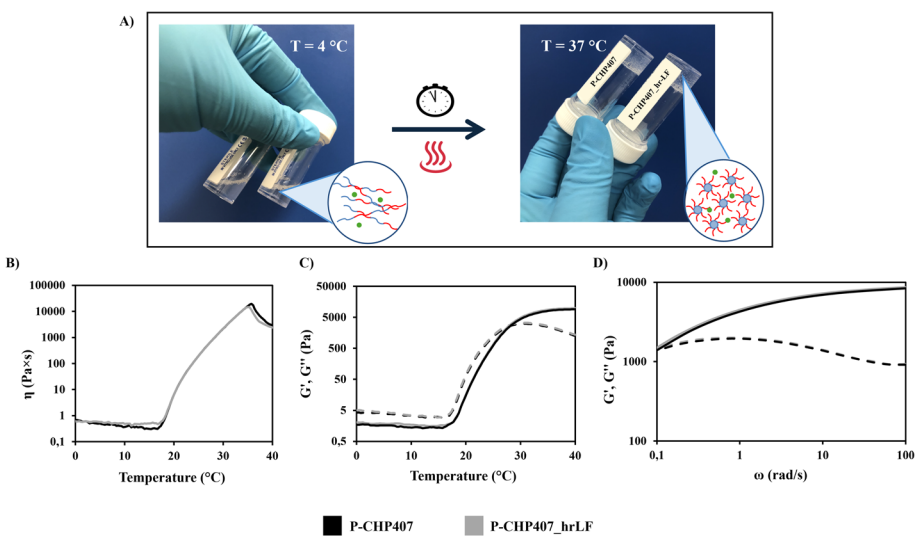

Fig. 1 (A) Macroscopic images of the unloaded- and hrLF-loaded -formulations undergoing gelation upon temperature increase. Rheological characterization was performed on the P-CHP407 (black) and P-CHP407_hrLF (grey) formulations to study the influence of hrLF encapsulation on the temperature-induced hydrogel gelation. (B) Continuous temperature ramp test showing the viscosity (η) changes as a function of the temperature in the range of 0 °C–40 °C. (C) Dynamic temperature ramp test showing the storage (G', continuous line) and loss (G'', dashed line) modulus profiles as a function of the temperature in the range of 0 °C–40 °C. (D) Frequency sweep test at 37 °C showing the G' and G'' moduli as a function of the angular frequency (ω) in the range of 0.1–100 rad s^{-1}.

lations, respectively. Lastly, the viscoelastic properties of the system at physiological temperature were studied through frequency sweep tests (Fig. 1D), which evidenced the attainment of a gel state (*i.e.*, $G' > G''$) at 37 °C for both systems, in accordance with dynamic temperature ramp test observations. Therefore, it was possible to conclude that the encapsulation of a high molecular weight protein did not alter the overall rheological properties of the PEU-based hydrogels.

Lactoferrin behaviour in contact with buffers

To avoid misinterpretations of drug release test results, potentially due to pH-dependent hrLF solubility and conformational changes in turn affecting its quantification, protein stability in buffers at pH values ranging between 5 and 11 was first studied for up to 7 days of incubation at 37 °C. For this purpose, two different approaches were exploited; namely, the absorbance measurement at 280 nm and the BCA colorimetric assay, since they underpin different working principles. Indeed, the former allows a direct detection of the protein, exploiting the signal at 280 nm ascribed to its aromatic ring; the latter involves indirect hrLF detection as a consequence of its interaction with BCA reagents, leading to a colour change from green to violet. Moreover, different detection sensitivities are associated with these tests, *i.e.*, protein concentrations in the range 0.1–0.4 mg mL^{-1} and 1–30 μg mL^{-1}, respectively.

Fig. 2 and 3 show the absorbance at 280 nm and 560 nm, respectively, measured for standard hrLF samples analysed as a function of time and pH upon incubation at physiological temperature. Concerning the investigation of hrLF stability through UV analyses (Fig. 2), very similar absorbance values were measured at each time point up to 7 days of incubation at 37 °C, irrespective of the considered pH buffer, meaning that the amount of detected hrLF remained almost constant over time. Therefore, these observations suggested the absence of protein degradation induced under both the pH condition and the long-term incubation at physiological temperature. Moreover, from a practical point of view, this result demonstrated the suitability of the curve obtained at time zero as a calibration curve for the quantification of the hrLF release from the hydrogels for up to 7 days. The investigation of hrLF stability carried out using the BCA assay (Fig. 3) further confirmed the previous observations, although the curves were not completely overlapped at each tested pH condition. Indeed, these slight differences could be ascribed to the higher sensitivity of the BCA assay compared to UV analyses, and the intrinsic error in the preparation of the samples, which requires the use of very small volumes and high dilution factors.

However, comparison of the curves obtained at time zero at different pH values by UV analyses (Fig. 4A) and the BCA assay (Fig. 4B) highlighted different hrLF behaviours based on the adopted testing approach. Indeed, UV analyses suggested that the measured absorbance values were independent of the buffer pH used for the dissolution of the protein. Conversely,

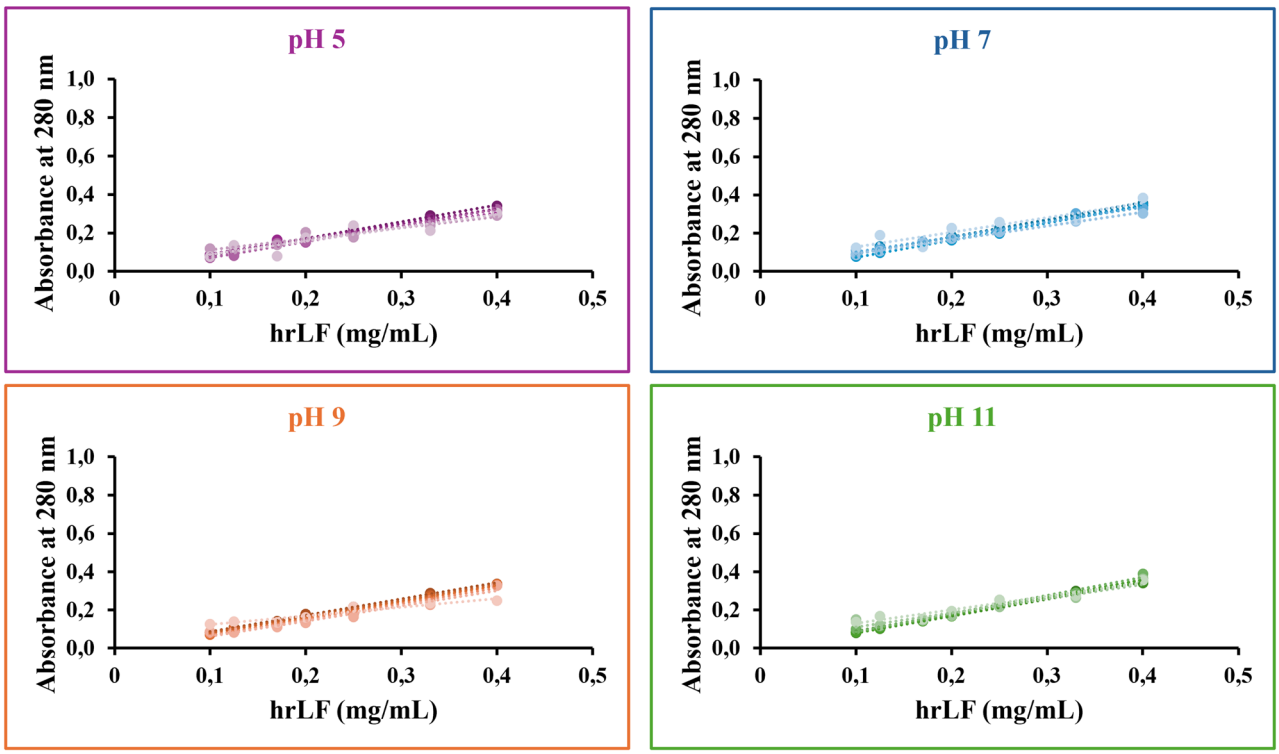

Fig. 2 Absorbance values measured at 280 nm by UV/Vis spectroscopy for the hrLF samples prepared by dissolving the protein at concentrations ranging from 0.1 to 0.4 mg mL^{-1} in buffers at pH 5 (violet), 7 (blue), 9 (orange) and 11 (green). For each considered pH, analyses were performed at t_0 and after 24 h, 48 h, 72 h, 96 h and 7 d (from dark to light colour) of incubation at 37 °C.

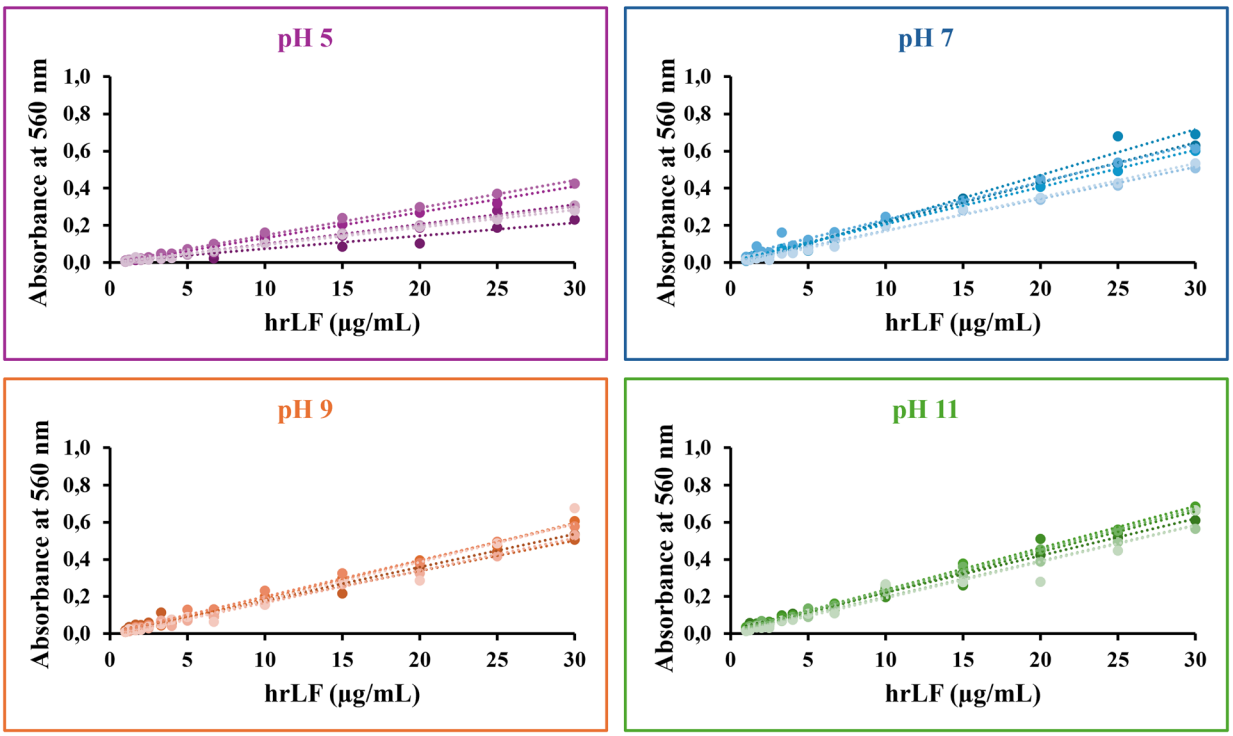

Fig. 3 Absorbance values at 560 nm obtained using the BCA assay performed on the hrLF samples prepared by dissolving the protein at concentrations ranging from 1 to 30 µg mL^{-1} in buffers at pH 5 (violet), 7 (blue), 9 (orange) and 11 (green). For each considered pH, analyses were performed at t_0 and after 24 h, 48 h, 72 h, 96 h and 7 d (from dark to light colour) of incubation at 37 °C.

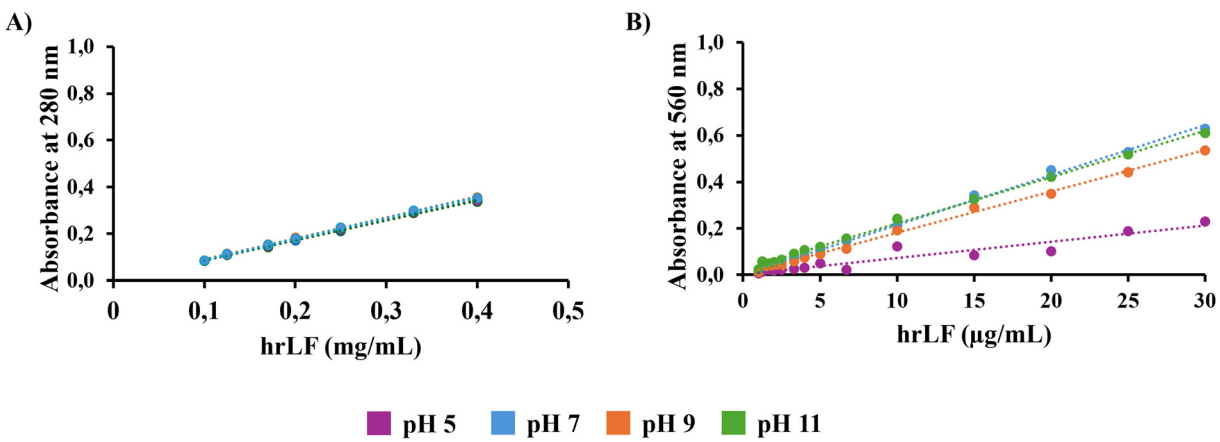

Fig. 4 Absorbance values measured at 280 nm (A) and 560 nm (B) for the standard samples prepared by dissolving the hrLF protein in buffers at pH 5 (violet), 7 (blue), 9 (orange) and 11 (green). Analyses were performed at time zero, *i.e.*, immediately after sample preparation.

the BCA assay evidenced a remarkable dependence between the registered absorbance and pH. Such observations could be explained by considering the slight pH-dependent solubility of hrLF[46] and the higher sensitivity of the BCA assay, compared to UV analyses, which allowed a more precise protein quantification. However, considering our purpose, this issue can be overcome by calculating drug release percentages at each pH by referring to the time-zero curve obtained at the corresponding pH. Moreover, although both approaches can be considered suitable for the quantification of hrLF, the BCA assay was selected for further studies due to its high sensitivity, which allowed a more precise and accurate protein detection.

Overall, hrLF showed a slight pH-dependent solubility and preserved its integrity when dissolved in fluids at different pH values and kept at physiological temperature for up to 7 days. Hence, it can be assumed that differences in the following *in vitro* drug release studies will not be affected by hrLF behaviour in buffers at different pH, but they will be exclusively due

to the ability of the hydrogel to tune the release kinetics in response to environmental conditions.

pH-controlled lactoferrin release

Considering that the engineered hrLF-loaded smart hydrogel was designed to work as an advanced chronic wound healing treatment, the investigation of its release capability in contact with fluids at different pH is of crucial importance. Indeed, the exudate produced by chronic wounds can show acidic or alkaline values depending on the clinical status. In more detail, the presence of persistent inflammation is usually associated with the production of acidic fluids;[47] conversely, bacterial contamination results in an alkaline exudate characterized by a different degree of alkalinity (generally between 7 and 9) based on the type of bacteria colonizing the wound bed.[37] Therefore, such clinical features associated with chronic wounds have been explored as triggering stimuli for the design of smart medicated wound dressings. In this context, the suitability of P-CHP407 hydrogels to work as smart drug delivery systems has already been demonstrated by studying their capability to release a low molecular weight anti-inflammatory drug (*i.e.*, ibuprofen) in response to pH 5 and 8.[39] Although promising results were obtained in that work, a higher degree of control over the pH-release mechanism should be proven to definitively demonstrate the superior effectiveness of the hydrogels as advanced delivery carriers. Therefore, in this work, P-CHP407 hydrogel performance was tested by considering pH values ranging from 5 to 11. Specifically, although the most clinically relevant pH values vary between 7 and 9, pH 11 was also included in this study to better investigate hydrogel pH-responsiveness and provide evidence of system suitability for applications requiring such alkaline environments. Moreover, an additional level of difficulty was introduced by studying the release mechanism of a high molecular weight protein in order to demonstrate the versatility of the carrier.

Fig. 5 shows the release of hrLF from P-CHP407 hydrogels in contact with buffers at pH 5, 7, 9 and 11 within the first 6 h of incubation at 37 °C (see Fig. S3 for hrLF release up to 7 days).

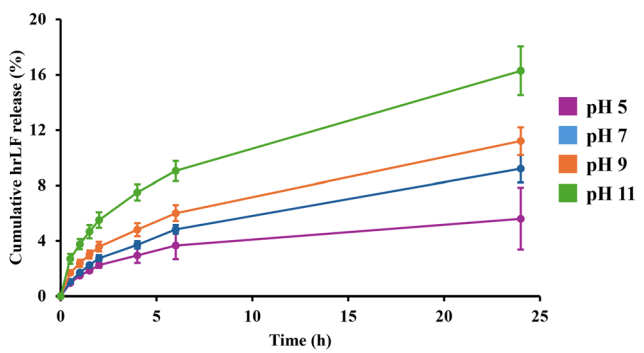

Fig. 5 *In vitro* hrLF release from the P-CHP407 hydrogels in contact with buffers at pH 5 (violet), 7 (blue), 9 (orange) and 11 (green) detected using the BCA colorimetric assay. Analyses were performed in quintuplicate, and data were analysed through two-way ANOVA followed by Šídák's multiple comparisons test.

Irrespective of the considered pH, sustained protein release was detected over time. Moreover, at each considered time point, increasing amounts of hrLF were detected by varying the fluid pH from acidic to alkaline. Such observations proved the capability of the P-CHP407 hydrogel network to release a high molecular weight protein and tune the release mechanism in response to an external stimulus through carboxylic acid group deprotonation in alkaline environments, leading to electrostatic polymeric chain repulsion and consequently, network enlargement,[39] even in the presence of more complex molecules such as hrLF.

Specifically, starting from 2 h of incubation, a significantly different hrLF release ($p < 0.01$) was detected from hydrogels in contact with buffer at pH 5 compared to pH 11. At 24 h, the released hrLF was quantified to be 5.6% ± 2.2%, 9.2% ± 0.9%, 11.3% ± 1.0% and 16.3% ± 1.7% from hydrogels against buffers at pH 5, 7, 9 and 11, respectively. Considering that the total encapsulated hrLF concentration was equal to 2 mg mL^{-1}, such percentages corresponded to 112 μg ± 45 μg, 184 μg ± 20 μg, 225 μg ± 20 μg and 326 μg ± 35 μg, respectively, which represent amounts exerting therapeutic effects.[48–50]

Concerning the release mechanism, data analysis within the first 7 h of incubation through the Korsmeyer-Peppas model gave release exponents equal to 0.54 ± 0.08, 0.61 ± 0.04, 0.51 ± 0.03 and 0.49 ± 0.05 for P-CHP407_hrLF hydrogels in contact with buffers at pH 5, 7, 9 and 11, respectively. Thus, irrespective of external pH, the systems showed a non-Fickian diffusion mechanism.[51] Indeed, considering the experimental uncertainty associated with the fitting procedure, the approximations of the model (*e.g.*, system showing planar geometry) and the concurrent occurrence of multiple phenomena (*e.g.*, swelling, electrostatic interactions), the obtained value at pH 11 should be regarded as a borderline case and can also be reasonably interpreted as anomalous. Such observed release mechanism is in contrast to the conclusions reached in our previous work, where it was described to be non-Fickian diffusion (*i.e.*, 0.52 ± 0.12) and Fickian diffusion transport (*i.e.*, 0.16 ± 0.01) for systems at pH 5 and 8, respectively.[39] However, although the carrier was the same (*i.e.*, P-CHP407 hydrogels), these studies differ with respect to the payload (*i.e.*, Ibuprofen *vs.* hrLF), which are characterized by extremely different features. Indeed, while Ibuprofen is a low molecular weight hydrophobic molecule, hrLF is a high molecular weight hydrophilic protein. Thus, it is reasonable to expect that they are located in different positions within the network (*i.e.*, ibuprofen in the hydrophobic micelle core, hrLF in the interstitial spaces among the micelles). Moreover, the payload molecular weight also plays a crucial role in network organization, probably leading to the formation of a higher mesh size in the presence of hrLF. In addition, hrLF also shows a positive superficial charge, which could interact with the negative charge of deprotonated carboxylic acid groups, strongly affecting the release mechanism (Fig. S4). Therefore, based on these differences, the release exponents macroscopically describing the release mechanism of Ibuprofen-loaded and hrLF-loaded systems could not be directly compared.

Lastly, hrLF released over 7 hours of incubation was also quantified by enzyme-linked immunosorbent assay (ELISA) in order to verify the absence of pH-induced hrLF conformational changes that are not directly detectable through the BCA colorimetric test (Fig. 6). This aspect is of crucial importance in terms of hrLF therapeutic activity. Indeed, the main mechanism underlying hrLF antimicrobial action deals with its iron-sequestering capability, which, in turn, is strictly dependent on protein large-scale structural conformation.[52] Therefore, conformational changes could potentially limit the iron-binding efficacy and, thus, the antimicrobial therapeutic effect exerted by the protein.

As shown in Fig. 6, the release profiles obtained at pH 5, 7 and 9 by the ELISA assay overlapped with those resulting from the BCA test, further proving the tunable release capability of P-CHP407 hydrogels in response to external pH and the consistency of the data derived from the colorimetric assay. Differently, at the highest tested pH condition (*i.e.*, pH 11), extremely different amounts of hrLF were quantified at each tested time point based on the adopted assay, indirectly suggesting the occurrence of potential protein conformational changes that limited the sensitivity of the ELISA-mediated quantification. Therefore, although the smart delivery system was effectively able to release higher amounts of therapeutic agent at pH 11 compared to lower environmental pH conditions, it is reasonable to argue that a potentially reduced therapeutic action is exerted in this condition. However, further investigations are required to directly prove that pH 11 induced hrLF conformational changes.

Cytocompatibility of hydrogel formulations

The cytocompatibility of the engineered formulation was first preliminarily assessed according to the ISO 10993:5 regulations. For this purpose, P-CHP407 and P-CHP407_hrLF hydrogels were incubated in contact with complete culture medium for 24 h, and then the extract-enriched medium was used to culture NIH-3T3 murine fibroblasts for an additional 24 h under normal culture conditions. The results showed high cell viability (>80%) and low cytotoxicity (<20%) percentages for both the unloaded and hrLF-loaded formulation, thus suggesting the absence of cytotoxic effects potentially induced by either the polymer or the encapsulated protein (Fig. 7). Moreover, fluorescent images acquired through the live and dead assay further confirmed these observations, proving the cytocompatibility of the hydrogel extracts.

Evaluation of lactoferrin cytocompatibility under drug-releasing conditions

Before studying the therapeutic actions exerted by the pH-released hrLF in the prospective treatment of chronic skin wounds, protein interaction with human dermal fibroblasts

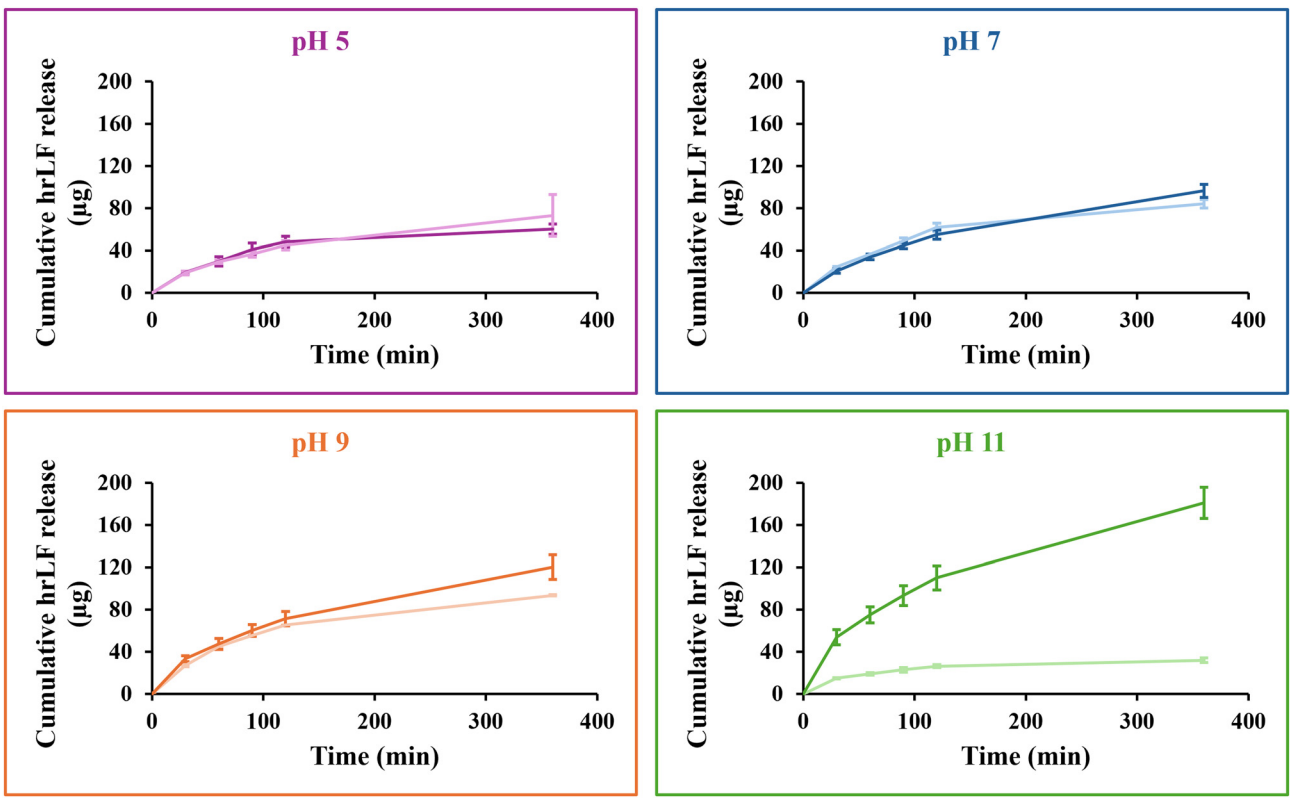

Fig. 6 hrLF released from the P-CHP407 hydrogels in contact with buffers at pH 5 (violet), 7 (blue), 9 (orange) and 11 (green) as quantified by the BCA colorimetric test (dark colours) and enzyme-linked immunosorbent assay (ELISA, light colours). Analyses were performed in triplicate, and data were analysed through two-way ANOVA, followed by Šídák's multiple comparisons test (pH 5: ns, pH 7: ns, pH 9: $0.001 < p < 0.01$ at 24 h, and pH 11: $p < 0.0001$) at each considered time point.

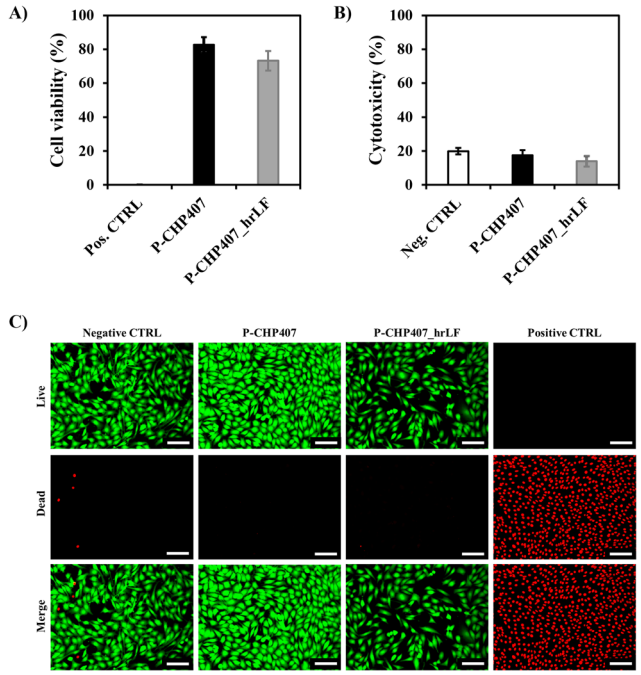

Fig. 7 Assessment of the hydrogel cytocompatibility according to the ISO 10993:5 regulations. Cell viability (A) and cytotoxicity (B) percentages calculated for the P-CHP407 and P-CHP407_hrLF formulations through the CellTiter-Blue and CytoTox-ONE assays, respectively. (C) Live and dead images of the NIH-3T3 cells cultured with P-CHP407 and P-CHP407_hrLF enriched extracts for 24 h. Live and dead cells are stained in green and red, respectively. Negative and positive controls correspond to the cells cultured in complete culture medium and lysed before the assay, respectively. Number of technical replicates: 5 and number of biological replicates: 3. No statistical differences were obtained by data analyses through two-way ANOVA, followed by Šídák's multiple comparisons test.

(HDFs) was first studied by analyzing cell metabolic activity up to 5 days of culture in the presence of hrLF (Fig. 8). For this purpose, hrLF concentration was varied in the range 10–500 μg mL^{-1} in order to encompass the entire interval of protein amounts released from 1 mL of hydrogels, as registered through the *in vitro* drug release test. Furthermore, a more in-depth evaluation was also conducted through the cell cycle assay performed on HDFs treated with the highest tested hrLF concentration (*i.e.*, 500 μg mL^{-1}) for the same time points (*i.e.*, 1 d, 2 d and 5 d) (Fig. 9).

Irrespective of tested hrLF concentration, HDFs were found to be metabolically active during the entire duration of the experiment. In more detail, percentages registered at day 1 and day 2 showed values very similar to those registered for the control (*i.e.*, cells cultured in hrLF-free medium - red line in the graph), thus suggesting the absence of protein-induced alterations of cell metabolism. Differently, at longer culture times (*i.e.*, 5 days), the metabolic activity of hrLF-treated cells was remarkably higher compared to that of the control, thus suggesting a capability of the protein to act as a cell proliferation-inducing agent.[53] This observation was especially evident for the highest tested hrLF concentration (*i.e.*, 500 μg mL^{-1}), with a metabolic activity percentage measured to be 136.5% ± 3.5%.

To gain a more in-depth understanding of the capacity of hrLF to stimulate cell metabolic activity (and consequently anticipate benefits in the treatment of chronic skin wounds achieving faster tissue healing), its interaction with the different cell phases was evaluated using the cell cycle assay (Fig. 9). To note, the assay was performed using actively proliferating cultures, in which the majority of cells were expected to be cycling under standard growth conditions. This approach was intentionally chosen to better mimic the physiological wound microenvironment, where cells are naturally distributed across different stages of the cell cycle rather than being synchronized in a single phase. The life cycle of eukaryotic cells encompasses four distinct phases: sub-G1, considered to be the resting phase in which cells exert their function or undergo apoptosis; G0/G1, ascribed to cell growth by first synthesizing RNA and proteins; S phase, attributed to DNA synthesis and thus cell proliferation; and G2/M, in which cells continue to grow and undergo nuclear and cytoplasmic division. At time 0 (*i.e.*, at the beginning of the experiment), most of the cells were found to be in the G0/G1 phase, meaning that they were normally growing before being seeded. At day 1, both untreated and hrLF-treated HDFs (Fig. 9A and B, respectively) showed a reduction in the G0/G1 phase in favour of S and G2/M phases, suggesting the re-establishment of cell-proliferating conditions. Afterwards, a progressive slight reduction in the proliferative and division phases was observed up to day 5 of culture due to the achievement of cell confluence. Specifically, this trend was registered for both the control and HDFs treated with hrLF, thus suggesting the absence of protein-induced alteration of the cell cycle. However, a closer analysis of the S phase (Fig. 9C) evidenced slightly higher cell percentages measured for HDFs treated with hrLF compared to control cells, at each analysed time point. For instance, at day 1, the percentages of cells in the S phase were measured to be 10.8% ± 1.6% and 12.7% ± 1.0% for untreated and hrLF-treated HDFs, respectively. These differences, although not statistically significant, align with evidence reported in the literature on the proliferative effect exerted by hrLF, probably through a synergistic action on the modulation of both fibroblast growth factor-2 and transforming growth factor-β1.[54]

Evaluation of lactoferrin pro-regenerative and anti-inflammatory activities under wound-mimicking conditions

HDFs pre-conditioned with 10 μg mL^{-1} LPS were used as a simplified experimental model of inflammation, and the anti-inflammatory effect of hrLF was investigated. As shown in Fig. 10A, the metabolic activity of LPS-treated HDFs was not affected by the inflammatory potential of LPS, reaching a cell viability higher than 100% over five days of culture. In fact, previous studies have shown stimulatory effects of LPS on HDF growth.[55–57] This dual effect arises because different cell types (*i.e.*, immune cells and fibroblasts) interpret LPS-triggered signals differently. Immune cells emphasize rapid cytokine release, whereas fibroblasts may respond by proliferating or

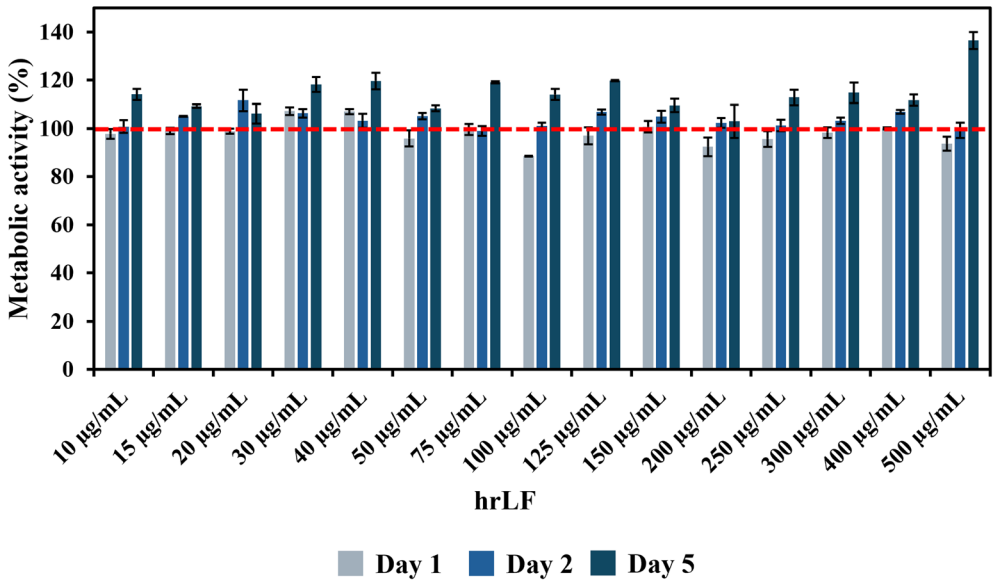

Fig. 8 Alamar Blue assay performed to evaluate the metabolic activity of the HDFs cultured with the hrLF-enriched media for 1 d, 2 d and 5 d. The results are expressed as percentages with respect to the negative control, *i.e.*, HDFs cultured in complete medium (red line). Number of technical replicates: 3 and number of biological replicates: 3. Data analysed through two-way ANOVA, followed by Šídák's multiple comparisons test, gave $p <$ 0.0001 at day 5 for each hrLF tested concentration except for 20 and 200 μg mL^{-1}.

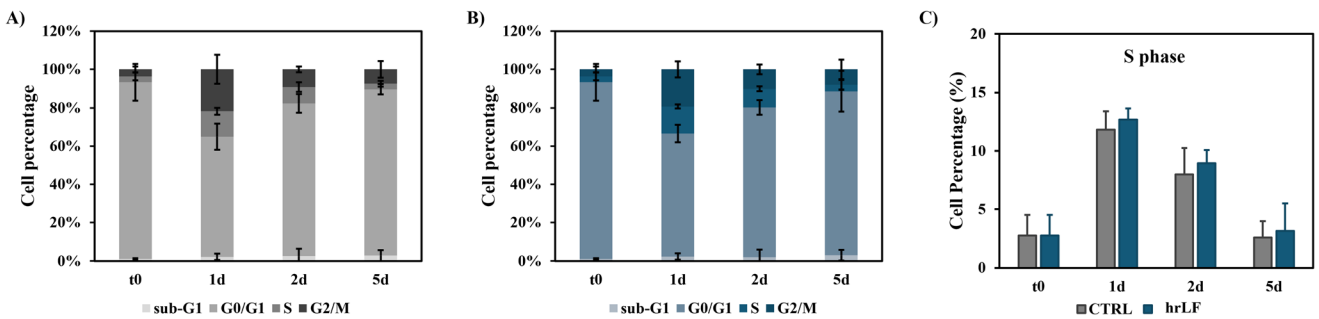

Fig. 9 Cell cycle assay performed on the untreated HDFs (A) and hrLF-treated HDFs (B). For this test, cells were treated with the highest tested hrLF concentration (*i.e.*, 500 μg mL^{-1}). Comparison of the cell percentages registered in the proliferation phase (S phase) for the untreated (grey) and hrLF-treated (blue) cells (C). Number of technical replicates: 3 and number of biological replicates: 3. Data analysed through two-way ANOVA, followed by Šídák's multiple comparisons test, gave no statistically significant differences.

activating ECM deposition.[58] The overall cellular outcome, however, is highly context-dependent and influenced by factors such as LPS concentration, exposure periods, presence of additional growth factors, and intercellular crosstalk.[59,60]

The treatment with hrLF at 100, 500, and 750 μg mL^{-1} positively influenced HDF viability, showing a trend of increasing metabolic activity over time. Specifically, the first two hrLF concentrations were selected to mimic the hrLF released after 24 h from 1 mL of hydrogel exposed to buffers at pH 5, 7, and 9, respectively; differently, 750 μg mL^{-1} was included to further investigate the potential therapeutic effect of the protein in view of its clinical translation, where larger application volumes and/or greater exposed surface areas may reasonably lead to higher local amounts of released hrLF over the same time interval. Cells treated with 100 μg mL^{-1} hrLF exhibited a viability increase from 109.2% ± 8.5% on day 1 to 118.2% ± 6.0% on day 5. A significant increase ($p^* < 0.05$) was observed for cells treated with 500 μg mL^{-1} hrLF, rising from 104.2% ± 8.6% on day 1 to 118.6% ± 5.1% on day 5. Similarly, treatment with 750 μg mL^{-1} hrLF resulted in a significant viability enhancement ($p^* < 0.05$), from 106.8% ± 8.0% on day 1 to 118.6% ± 6.9% on day 5. These findings confirm hrLF's protective and stimulatory role under inflammatory stress, consistent with literature reporting that lactoferrin potentiates fibroblast viability and tissue integrity during inflammation.[61,62]

Quantitative analysis of double-stranded DNA (dsDNA) further confirmed the mitogenic effect of hrLF (Fig. 10B). Confirming the stimulatory effects of LPS on HDF behavior, a similar proliferation rate was observed between the unstimulated control group (CTRL) and LPS-treated cells, showing a

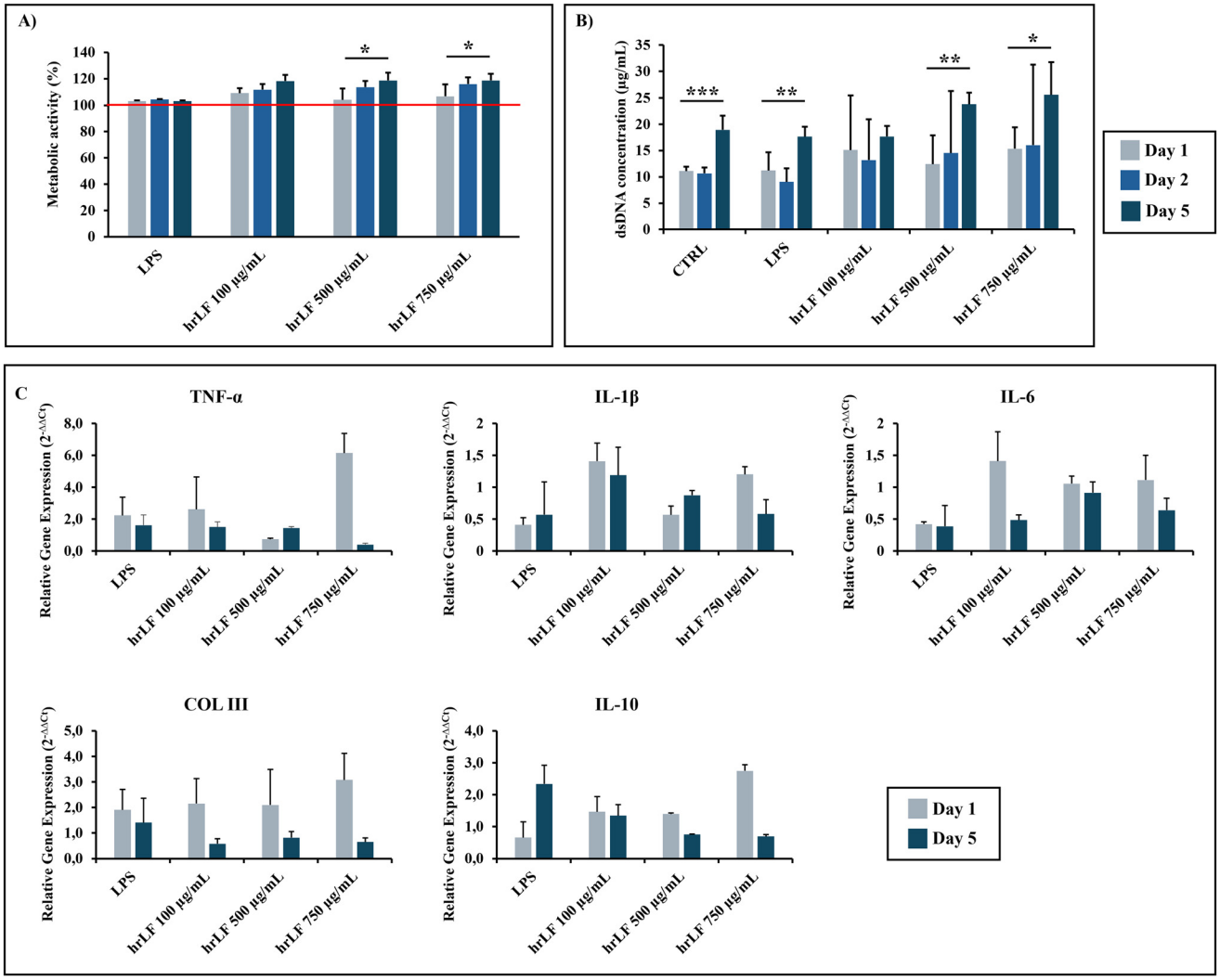

Fig. 10 Evaluation of the hrLF anti-inflammatory and pro-regenerative activities under wound-mimicking conditions. Metabolic activity (A) and dsDNA quantification (B) of the HDFs pre-conditioned with LPS and after treatment with hrLF at increasing concentrations (100, 500 and 750 µg mL^{-1}). Number of technical replicates: 3 and number of biological replicates: 3. Gene expression profile of the pro-inflammatory (TNF-α, IL-1β, and IL-6), anti-inflammatory (IL-10) and pro-regenerative (COL III) markers on the LPS-conditioned HDFs treated with hrLF at increasing concentrations (100, 500 and 750 µg mL^{-1}) (C). Number of technical replicates: 2 and number of biological replicates: 3. Data were analysed through two-way ANOVA, followed by Šídák's multiple comparisons test. ***: $0.0001 < p < 0.001$, **: $0.001 < p < 0.01$, and *: $0.01 < p < 0.05$.

significant increase in cell proliferation from day 1 to day 5 ($p^{***} < 0.001$ and $p^{**} < 0.01$, respectively). Similarly, a significant increase in DNA content was observed from day 1 to day 5 in cells treated with hrLF at 500 µg mL^{-1} ($p^{**} < 0.01$) and 750 µg mL^{-1} ($p^{*} < 0.05$). As expected, these hrLF-treated cells (500 µg mL^{-1} and 750 µg mL^{-1}) showed on day 5 a tendency for higher DNA levels than both LPS-treated cells and the CTRL group, confirming the regenerative potential of lactoferrin beyond mere inflammation suppression.[61,62]

The gene expression profile revealed that hrLF treatment markedly reduced the LPS-induced expression of pro-inflammatory cytokines TNF-α, IL-1β, and IL-6 in HDFs (Fig. 10C).

A pronounced suppression was observed with 100 µg mL^{-1} and 750 µg mL^{-1} hrLF, which aligns with literature reporting that LPS-treated HDFs exposed to LF ranging between 10–300 µg mL^{-1} reduced IL-1β and IL-6 expression.[63] Colonic fibroblasts also lowered TNF-α, IL-1β, and IL-6 expression when treated with LF at micromolar levels.[61] Different reviews also show that LF can reduce the expression of TNF-α, IL-1β, and IL-6 in macrophages and epithelial cells treated with LF (≤100–500 µg mL^{-1}).[64] This anti-inflammatory effect of LF is primarily attributed to its capacity to bind and neutralize LPS, thereby preventing its interaction with the TLR4–MD2–CD14 receptor complex and the subsequent activation of NF-κB and MAPK (p38/JNK) signaling pathways.[65] By maintaining NF-κB in an inactive state and limiting MAPK phosphorylation, LF downregulates the transcription of cytokine genes such as TNF-α, IL-1β, and IL-6. Comparable findings were reported for LPS-treated HDFs, where LF reduced IL-1β and IL-6 expression *via* inhibition of the JNK pathway.[66] Interestingly, increasing

levels of hrLF decreased IL-10 expression, an anti-inflammatory marker, following LPS stimulation. Although IL-10 expression is regulated by signalling pathways that are not exclusively dependent on NF-κB, the reduction in IL-10 observed with increasing hrLF concentration may be an indirect consequence of hrLF-mediated suppression of TNF-α, a major inducer of IL-10 production in LPS-stimulated monocytes.[67–69] These findings are consistent with reports showing reduced IL-10 levels in hrLF-treated monocyte cell lines.[70]

Regarding collagen type III (COL III) expression, an early marker of wound healing and fibrosis, it was downregulated across all hrLF treatment groups. This is notable given that LPS is known to upregulate collagen production in fibroblasts, a response associated with hypertrophic scarring.[71] Thus, the observed reduction in COL III by hrLF suggests a response to the LPS effects aimed at normalizing ECM remodeling, minimizing fibrosis, and promoting balanced wound repair.

Overall, our results indicate that under these testing conditions, hrLF exerts dual anti-inflammatory and pro-regenerative effects on HDFs by maintaining cell viability, enhancing proliferation, and regulating gene expression. These findings reinforce the concept that fibroblasts are not merely structural cells but also active participants in the innate immune response, capable of responding to therapeutic agents and potentially contributing to the resolution of inflammation and tissue repair.

Evaluation of lactoferrin antimicrobial properties

The antimicrobial activity of hrLF was evaluated against representative Gram-positive (*Staphylococcus aureus*) and Gram-negative (*Escherichia coli*) bacterial strains, which are both key pathogens in chronic wounds due to their persistence, biofilm-forming capacity, and resistance to antibiotic treatment (Fig. 11). The results demonstrated a pronounced bacteriostatic effect for *S. aureus*, with hrLF significantly reducing the number of viable colonies at 6 h of incubation compared to control cultures. Between 6 and 24 h, bacterial counts were reduced, although without significant differences. In contrast, hrLF exhibited weaker activity against *E. coli*, causing only a transient reduction in bacterial counts within the first hours, with no significant long-term effect compared to controls. These findings are consistent with previous studies reporting that lactoferrin can exert a microbiostatic activity against both Gram-positive and Gram-negative bacteria.[72,73] Lactoferrin's antimicrobial function is attributed to the following mechanisms of action: (i) a bacteriostatic effect through iron chelation, which limits microbial growth by depriving bacteria of this essential nutrient, and (ii) bactericidal activity mediated by its cationic N-terminal peptide, lactoferricin, which disrupts microbial membranes.[74,75] However, the nature and magnitude of these effects depend on several factors, including the form of lactoferrin, its concentration, the bacterial strain, and the duration of exposure.

In our study, the observed bacteriostatic effect of hrLF is consistent with the first mechanism, as bacterial viability was reduced without evidence of complete eradication. The higher sensitivity of *S. aureus* compared with *E. coli* may be explained by differences in cell envelope architecture: the absence of an outer membrane in Gram-positive bacteria facilitates iron deprivation effects, whereas the outer membrane of Gram-negative bacteria provides an additional protective barrier that can limit hrLF activity. Nonetheless, the reduction in bacterial viability in both strains highlights the broad antimicrobial potential of hrLF, albeit with species-dependent efficacy.

Taken together, these results confirm the antibacterial potential of hrLF and highlight its therapeutic relevance for potentially treating chronic wounds. Beyond its bacteriostatic role, lactoferrin has been reported to act synergistically with antibiotics and host defence peptides, potentially reducing the risk of resistance development.[76] Thus, hrLF-loaded hydrogels may offer a

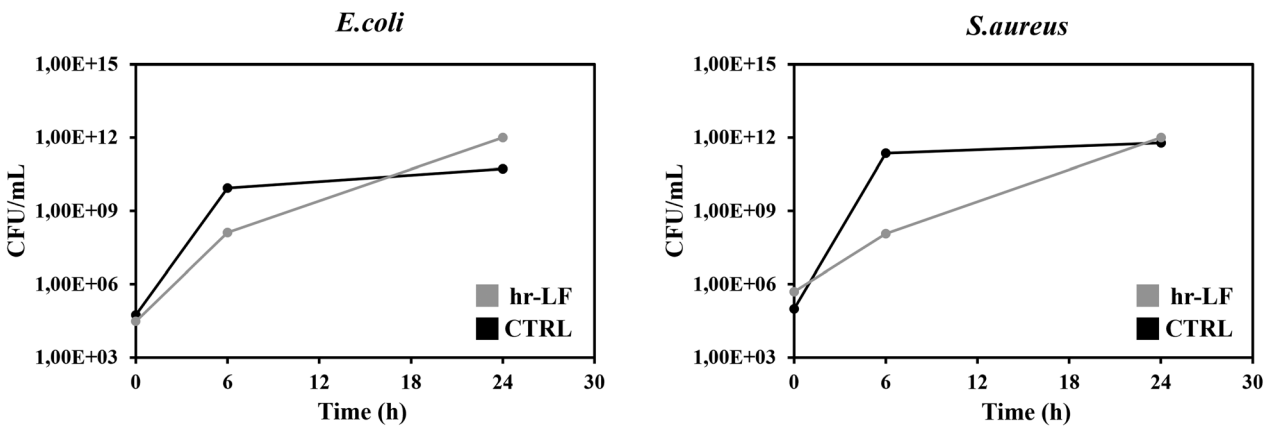

Fig. 11 Antimicrobial activity of hrLF against *Staphylococcus aureus* and *Escherichia coli*. Bacterial counts were quantified over time in cultures in the absence (CTRL) and presence of hrLF. Results are presented as mean ± standard deviation from three independent experiments. Number of technical replicates: 3 and number of biological replicates: 3. Data analysed through two-way ANOVA, followed by Šídák's multiple comparisons test, gave $0.0001 < p < 0.001$ at 6 h for *S. aureus* and $0.001 < p < 0.01$ at 6 h and 24 h for *E. coli*.

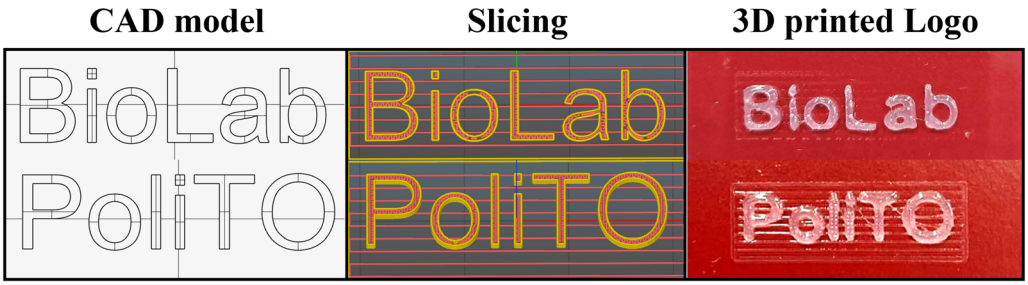

Fig. 12 Representation of the P-CHP407_hrLF hydrogel extrusion into 3D structures: virtual model design, conversion into printing instructions and logo fabrication (from left to right).

dual benefit of antimicrobial protection and promotion of tissue regeneration, making them promising candidates for the management of infected and inflamed hard-to-heal wounds.

Hydrogel processability through 3D bioprinting

In view of hydrogel processing in the form of patient-personalized wound dressings, a proof-of-concept of P-CHP407_hrLF hydrogel suitability as a biomaterial ink was obtained by extruding different 3D logo representations by setting processing parameters optimized in a different work (data not reported) (Fig. 12). For this purpose, the formulation was loaded into a cartridge at low temperature, equilibrated at 22 °C to ensure the achievement of a semi-gel state, and then deposited on a previously equilibrated printing bed at physiological temperature. Each logo resulted from the layer-by-layer deposition of five consecutive layers. Since the extruded structures finely reproduced the corresponding virtual models, this preliminary qualitative experiment further proved the thermoresponsiveness of the system and the capability to temperature-control the extrusion process and construct shape retention over time. Further studies will be performed to investigate the stability of 3D printed structures in contact with fluids and to optimize the printing parameters, allowing the fabrication of complex shape-personalized patches.

Conclusions

The lack of patient-personalization characterizing the currently available wound dressings for chronic skin wound management remains the main limitation hindering tissue healing. This work describes the engineering of a smart formulation with potential for patient-specific treatment of chronic skin wounds. Specifically, the synthesis of a multi-stimuli-responsive poly(ether urethane) allowed the formulation of a thermo- and alkaline-pH responsive hydrogel capable of encapsulating a high molecular weight protein with no changes in the thermal behavior, with release of payload in response to patient's clinical needs. In addition, hrLF has proved to be a suitable therapeutic agent that can preserve its conformation even in the harsh wound environment. Moreover, amounts of hrLF defined according to drug release profiles showed the capability to promote tissue regeneration, reduce inflammation, and exert bacteriostatic activity when tested in an *in vitro* model of simplified wound inflammation. Finally, a first assessment was able to demonstrate the hydrogel extrudability and shape retention capability after extrusion, paving the way for the fabrication of shape-personalized wound dressings. Based on these promising results, future investigations will be focused on the assessment of system performance in a more clinically relevant environment (*e.g.*, 3D wound models encompassing the co-culture of fibroblasts, keratinocytes and macrophages). Moreover, future steps will address challenges towards the translation of this proof-of-concept system into a clinically applicable wound dressing, such as the development of a scalable and reproducible polymer synthesis process, compliance with Good Manufacturing Practice (GMP) requirements, and the assessment of the long-term physicochemical and biological stability of the final formulation under storage conditions. In addition, manufacturing consistency, sterilization procedures, and shelf-life validation will be crucial to ensure product quality and regulatory approval.

Author contributions

Rossella Laurano: conceptualization, investigation, writing – original draft, methodology, validation, visualization, formal analysis, data curation; Viviana Pinto Ribeiro: investigation, methodology, writing – original draft, validation, formal analysis, data curation; Cláudia S. Oliveira: investigation, writing – original draft, methodology, validation, formal analysis, data curation; Alessandro Torrisi: investigation, formal analysis, data curation, writing – review and editing; Alessandro Ligas: investigation, formal analysis, data curation, writing – review and editing; Monica Boffito: writing – review and editing, conceptualization; Freni K. Tavaria: writing – review and editing, supervision, resources; Ana Leite Oliveira: resources, writing – review and editing, supervision; and Gianluca Ciardelli: funding acquisition, writing – review and editing, supervision, resources.

Conflicts of interest

There are no conflicts to declare.

Data availability

The data supporting this article are available upon request to the authors.

Chemical characterization of untreated- and plasma-treated poly(ether urethane); drug release test and schematic representation of pH-controlled release mechanism. Supplementary information (SI) is available. See DOI: https://doi.org/10.1039/d6bm00877a.

Acknowledgements

This study was carried out within the HERO project–funded by the European Union–Next Generation EU within the PRIN 2022 program (D.D. 104-02/02/2022 Ministero dell'Università e della Ricerca). This research article reflects only the authors' views and opinions and the Ministry cannot be considered responsible for them. R. L. acknowledges the funding from the PON "Ricerca ed Innovazione" DM 1062/2021. This work was also supported by national funds from the Fundação para a Ciência e a Tecnologia (FCT) through the projects UIDB/50016/2020, 2023.07374.CEECIND, 2023.11204.PEX and 2024.05237.RESTART and by the project 0072_IBEROS_MAIS_1_E, Xunta de Galicia.

References

1 P. Schilrreff and U. Alexiev, *Int. J. Mol. Sci.*, 2022, **23**, 4928, DOI: 10.3390/ijms23094928.
2 J. Wang, *Cell Tissue Res.*, 2018, **371**, 531–539.
3 L. Cañedo-Dorantes and M. Cañedo-Ayala, *Int. J. Inflam.*, 2019, 3706315.
4 L. T. Marton, E. S. L. M. Pescinini, M. E. C. Camargo, S. M. Barbalho, J. Haber, R. V. Sinatora, C. R. P. Detregiachi, R. J. S. Girio, D. V. Buchaim and P. Cincotto Dos Santos Bueno, *Front. Endocrinol.*, 2021, **12**, 669448.
5 D. J. Yang, S. H. Moh, D. H. Son, S. You, A. W. Kinyua, C. M. Ko, M. Song, J. Yeo, Y. H. Choi and K. W. Kim, *Molecules*, 2016, **21**, 899.
6 Y. K. Bashmakov, S. H. Assaad-Khalil, M. Abou Seif, R. Udumyan, M. Megallaa, K. H. Rohoma, M. Zeitoun and I. M. Petyaev, *ISRN Endocrinol.*, 2014, **2014**, 816307.
7 M. Unlü, D. Daferera, E. Dönmez, M. Polissiou, B. Tepe and A. Sökmen, *J. Ethnopharmacol.*, 2002, **83**, 117–121.
8 P. C. Braga, M. Dal Sasso, M. Culici, T. Bianchi, L. Bordoni and L. Marabini, *Pharmacology*, 2006, **77**, 130–136.
9 M. Costa, A. Durço, T. K. Rabelo, R. Siqueira and A. Guimarães, *J. Pharm. Pharmacol.*, 2018, **71**, 141–155.
10 M. A. Neag, A. Mocan, J. Echeverría, R. M. Pop, C. I. Bocsan, G. Crişan and A. D. Buzoianu, *Front. Pharmacol.*, 2018, **9**, 557.
11 R. Zhou, C. Xiang, G. Cao, H. Xu, Y. Zhang, H. Yang and J. Zhang, *Clin. Sci.*, 2021, **135**, 613–627.
12 E. K. Kim, E. K. Jeong, S. B. Han and J. Hong, *Bull. Korean Chem. Soc.*, 2011, **32**, 3597–3602.
13 J. Huang, L. Chen, Z. Gu and J. Wu, *J. Biomed. Nanotechnol.*, 2019, **15**, 1357–1370.
14 B. B. Aggarwal, C. Sundaram, S. Prasad and R. Kannappan, *Biochem. Pharmacol.*, 2010, **80**, 1613–1631.
15 M. L. Kruzel, M. Zimecki and J. K. Actor, *Front. Immunol.*, 2017, **8**, 1438, DOI: 10.3389/fimmu.2017.01438.
16 M. Sienkiewicz, A. Jaśkiewicz, A. Tarasiuk and J. Fichna, *Crit. Rev. Food Sci. Nutr.*, 2022, **62**, 6016–6033, DOI: 10.1080/10408398.2021.1895063.
17 X. Li, W. Zhang, W. Yu, Y. Yu, H. Cheng, Y. Lin, J. Feng, M. Zhao and Y. Jin, *Sci. Rep.*, 2025, **15**, 9965, DOI: 10.1038/s41598-025-90685-x.
18 T. Siqueiros-Cendon, S. Arevalo-Gallegos, B. F. Iglesias-Figueroa, I. A. Garcıa-Montoya, J. Salazar-Martınez and Q. Rascon-Cruz, *Acta Pharmacol. Sin.*, 2014, **35**, 557–566, DOI: 10.1038/aps.2013.200.
19 K. Okubo, M. Kamiya, Y. Urano, H. Nishi, J. M. Herter, T. Mayadas, D. Hirohama, K. Suzuki, H. Kawakami, M. Tanaka, M. Kurosawa, S. Kagaya, K. Hishkawa, M. Nangaku, T. Fujita, M. Hayashi and J. Hirahashi, *EBioMedicine*, 2016, **10**, 204–215, DOI: 10.1016/j.ebiom.2016.07.012.
20 S. Sabra and M. M. Agwa, *Int. J. Biol. Macromol.*, 2020, **164**, 1046–1060, DOI: 10.1016/j.ijbiomac.2020.07.167.
21 N. Ostan, A. Morgenthau, R. H. Yu, S. D. Gray-Owen and A. B. Schryvers, *Biochem. Cell Biol.*, 2017, **95**, 5–11, DOI: 10.1139/bcb-2016-0055.
22 W. Zhang, J. Hu, H. Wu, X. Lin and L. Cai, *APL Mater.*, 2025, **13**, 010601, DOI: 10.1063/5.0245545.
23 H. Xin, D. S. A. Al Maruf, F. Akin-Ige and S. Amin, *Emergent Mater.*, 2025, **8**, 1339–1356, DOI: 10.1007/s42247-024-00930-8.
24 J. H. Choi, J. S. Lee, D. H. Yang, H. Nah, S. J. Min, S. Y. Lee, J. H. Yoo, H. J. Chun, H. J. Moon, Y. K. Hong, D. N. Heo and I. K. Kwon, *ACS Omega*, 2023, **8**, 44076–44085.
25 A. Fathi, M. Gholami, H. Motasadizadeh, A. Malek-Khatabi, R. Sedghi and R. Dinarvand, *Carbohydr. Polym.*, 2024, **331**, 121856, DOI: 10.1016/j.carbpol.2024.121856.
26 H. Meng, J. Su, Q. Shen, W. Hu, P. Li, K. Guo, X. Liu, K. Ma, W. Zhong, S. Chen, L. Ma, Y. Hao, J. Chen, Y. Jiang, L. Li, X. Fu and C. Zhang, *Adv. Healthcare Mater.*, 2025, **14**, 2404966, DOI: 10.1002/adhm.202404966.
27 N. Li, A. Zhan, Y. Jiang and H. Liu, *Int. J. Biol. Macromol.*, 2022, **222**, 1551–1559, DOI: 10.1016/j.ijbiomac.2022.09.185.
28 Y. Wu, Y. Wang, L. Long, C. Hu, Q. Kong and Y. Wang, *J. Controlled Release*, 2022, **341**, 147–165, DOI: 10.1016/j.jconrel.2021.11.027.
29 H. Zhao, J. Huang, Y. Li, X. Lv, H. Zhou, H. Wang, Y. Xu, C. Wang, J. Wang and Z. Liu, *Biomaterials*, 2020, **258**, 120286, DOI: 10.1016/j.biomaterials.2020.120286.
30 C. Shi, Y. Zhang, G. Wu, Z. Zhu, H. Zheng, X. Sun, Y. Heng, S. Pan, H. Xiu, J. Zhang, Z. Yin, Z. Yu and B. B. Liang, *Adv. Healthcare Mater.*, 2024, **13**, e2302626, DOI: 10.1002/adhm.202302626.

31 X. Zhou, N. Xiaoqun, C. Yiwen, C. Haoxun, L. Daohuan, P. Dating, G. Zhijie, Z. Zhiwen, G. Cuiping, H. Jun, Y. Shan and G. Huilong, *ACS Mater. Lett.*, 2023, **5**, 3142–3155, DOI: 10.1021/acsmaterialslett.3c00925.

32 Y. Jing, T. Huang, B. Zhao, L. Zhao, N. Zhang, K. Zhang, K. Wang, J. Wang, J. Hua and Q. Tu, *Chem. Eng. J.*, 2024, **487**, 150561, DOI: 10.1016/j.cej.2024.150561.

33 Z. Xu, G. Liu, J. Huang and J. Wu, *ACS Appl. Mater. Interfaces*, 2022, **14**, 7680–7689, DOI: 10.1021/acsami.1c2346.

34 R. Laurano, M. Boffito, G. Ciardelli and V. Chiono, *Eng. Regener.*, 2022, **3**, 182–200, DOI: 10.1016/j.engreg.2022.04.002.

35 S. Ono, R. Imai, Y. Ida, D. Shibata, T. Komiya and H. Matsumura, *Burns*, 2015, **41**, 820–824, DOI: 10.1016/j.burns.2014.10.023.

36 L. A. Wallace, L. Gwynne and T. Jenkins, *Ther. Delivery*, 2019, **10**, 719–735, DOI: 10.4155/tde-2019-0066.

37 D. G. Metcalf, M. Haalboom, P. G. Bowler, C. Gamerith, E. Sigl, A. Heinzle and M. W. M. Burnet, *Wound Med.*, 2019, **26**, 100166, DOI: 10.1016/j.wndm.2019.100166.

38 R. Laurano, M. Boffito, A. Torchio, C. Cassino, V. Chiono and G. Ciardelli, *Polymers*, 2019, **11**, 2109, DOI: 10.3390/polym11122109.

39 R. Laurano, M. Boffito, M. Abrami, M. Grassi, A. Zoso, V. Chiono and G. Ciardelli, *Bioact. Mater.*, 2021, **6**, 3013–3024, DOI: 10.1016/j.bioactmat.2021.01.003.

40 R. Laurano, M. Abrami, M. Grassi, G. Ciardelli, M. Boffito and V. Chiono, *Front. Mater.*, 2020, **7**, 594515, DOI: 10.3389/fmats.2020.594515.

41 R. Laurano, M. Boffito, C. Cassino, L. Midei, R. Pappalardo, V. Chiono and G. Ciardelli, *Materials*, 2023, **16**, 2024, DOI: 10.3390/ma16052024.

42 R. Laurano, A. Torchio, G. Ciardelli and M. Boffito, *Gels*, 2023, **9**, 731, DOI: 10.3390/gels9090731.

43 R. Laurano, V. Chiono, C. Ceresa, L. Fracchia, A. Zoso, G. Ciardelli and M. Boffito, *Eng. Regener.*, 2021, **2**, 263–278, DOI: 10.1016/j.engreg.2021.12.001.

44 M. Feldo, M. Wójciak, A. Ziemlewska, S. Dresler and I. Sowa, *Molecules*, 2022, **27**, 4264, DOI: 10.3390/molecules27134264.

45 R. Laurano and M. Boffito, *Front. Bioeng. Biotechnol.*, 2020, **8**, 708, DOI: 10.3389/fbioe.2020.00708.

46 B. L. Álvarez-Mayorga, S. Romero-Gómez, J. L. Rosado, J. Ocampo-Hernández, J. Gómez-Guzmán and L. Ortiz-Frade, *Molecules*, 2024, **29**, 491, DOI: 10.3390/molecules29020491.

47 M. Malone, T. Bjarnsholt, A. J. McBain, G. A. James, P. Stoodley, D. Leaper, M. Tachi, G. S. Schultz, T. Swanson and R. D. Wolcott, *J. Wound Care*, 2017, **26**, 20–25, DOI: 10.12968/jowc.2017.26.1.20.

48 C. P. J. M. Brouwer, M. Rahman and M. M. Welling, *Peptides*, 2011, **32**, 1953–1963, DOI: 10.1016/j.peptides.2011.07.017.

49 X. Zhao, M. Kruzel, S. M. Ting, G. Sun, S. I. Savitz and J. Aronowski, *J. Cereb. Blood Flow Metab.*, 2021, **41**, 53–66, DOI: 10.1177/0271678X20925667.

50 H. Y. Guo, L. Jiang, S. A. Ibrahim, L. Zhang, H. Zhang, M. Zhang and F. Zheng Ren, *J. Nutr.*, 2009, **139**, 958–964, DOI: 10.3945/jn.108.100586.

51 S. Dash, P. N. Murthy, L. Nath and P. Chowdhury, *Acta Pol. Pharm.*, 2010, **67**, 217–223.

52 H. M. Baker and E. N. Baker, *Biochem. Cell Biol.*, 2012, **90**, 320–328, DOI: 10.1139/o11-071.

53 X. Li, W. Zhang, W. Yu, Y. Yu, H. Cheng, Y. Lin, J. Feng, M. Zhao and Y. Jin, *Sci. Rep.*, 2025, **15**, 9965, DOI: 10.1038/s41598-025-90685-x.

54 L. Tang, T. Cui, J. J. Wu, W. Liu-Mares, N. Huang and J. Li, *Wound Repair Regen.*, 2010, **18**, 123–131, DOI: 10.1111/j.1524-475X.2009.00563.x.

55 H. Yang, M. Kaneko, C. He, M. A. Hughes and G. W. Cherry, *Phytother. Res.*, 2002, **16**, 43–47, DOI: 10.1002/ptr.912.

56 Z. Xi, C. Y. Xie and Y. B. Xi, *BMC Musculoskelet. Disord.*, 2016, **17**, 43, DOI: 10.1186/s12891-016-0895-0.

57 J. B. Acosta, D. G. del Barco, D. C. Vera, W. Savigne, P. Lopez-Saura, G. G. Nieto and G. S. Schultz, *Int. Wound J.*, 2008, **5**, 530–539, DOI: 10.1111/j.1742-481X.2008.00457.x.

58 N. X. Landén, D. Li and M. Ståhle, *Cell. Mol. Life Sci.*, 2016, **73**, 3861–3885, DOI: 10.1007/s00018-016-2268-0.

59 Q. Xu, S. Mei, F. Nie, Z. Zhang, J. Feng, J. Zhang, X. Qian, Y. Gao, Z. He and S. Xing, *Lab. Invest.*, 2022, **102**, 432–439, DOI: 10.1038/s41374-021-00701-7.

60 Y. K. Kim, J. H. Hwang and H. T. Lee, *Innate Immun.*, 2022, **28**, 122–129, DOI: 10.1177/17534259221100170.

61 Y. Pan, Z. Liu, Y. Wang, L. Zhang, N. Chua, L. Dai, J. Chen and C. L. Ho, *Front. Bioeng. Biotechnol.*, 2021, **9**, 779018, DOI: 10.3389/fbioe.2021.779018.

62 T. Odatsu, S. Kuroshima, A. Shinohara, A. Valanezhad and T. Sawase, *Int. J. Biol. Macromol.*, 2021, **190**, 368–374, DOI: 10.1016/j.ijbiomac.2021.08.214.

63 C. H. Cheng, W. J. Hong, C. N. Li, Y. H. Huang, J. H. Tsai, C. Y. Huang, J. C. Wu, C. Y. Kuo and W. C. Kuo, *Curr. Issues Mol. Biol.*, 2025, **47**, 549, DOI: 10.3390/cimb47070549.

64 M. L. Kruzel, M. Zimecki and J. K. Actor, *Front. Immunol.*, 2017, **8**, 1438, DOI: 10.3389/fimmu.2017.01438.

65 D. Legrand, E. Elass, M. Carpentier and J. Mazurier, *Cell. Mol. Life Sci.*, 2005, **62**, 2549, DOI: 10.1007/s00018-005-5370-2.

66 H. Rao, X. Song, J. Lei, P. Lu, G. Zhao, X. Kang, D. Zhang, T. Zhang, Y. Ren, C. Peng, Y. Li, J. Pei and Z. Cao, *Int. J. Mol. Sci.*, 2022, **23**, 13478, DOI: 10.3390/ijms232113478.

67 K. W. Moore, R. de Waal Malefyt, R. L. Coffman and A. O'Garra, *Annu. Rev. Immunol.*, 2001, **19**, 683–765, DOI: 10.1146/annurev.immunol.19.1.683.

68 C. Wanidworanun and W. Strober, *J. Immunol.*, 1993, **151**, 6853–6861.

69 A. D. Foey, S. L. Parry, L. M. Williams, M. Feldmann, B. M. J. Foxwell and F. M. Brennan, *J. Immunol.*, 1998, **160**, 920–928, DOI: 10.4049/jimmunol.160.2.920.

70 L. Håversen, B. G. Ohlsson, M. Hahn-Zoric, L.Å Hanson and I. Mattsby-Baltzer, *Cell. Immunol.*, 2002, **220**, 83–95, DOI: 10.1016/S0008-8749(03)00006-6.

71 H. Yang, C. Hu, F. Li, L. Liang and L. Liu, *IUBMB Life*, 2013, **65**, 526–532, DOI: 10.1002/iub.1159.

72 A. Aguila, A. G. Herrera, D. Morrison, B. Cosgrove, A. Perojo, I. Montesinos, J. Pérez, G. Sierra, C. G. Gemmell and J. H. Brock, *FEMS Immunol. Med. Microbiol.*, 2001, **31**, 145–152, DOI: 10.1111/j.1574-695X.2001.tb00511.x.

73 H. Flores-Villaseñor, A. Canizalez-Román, M. Reyes-Lopez, K. Nazmi, M. de la Garza, J. Zazueta-Beltrán, N. León-Sicairos and J. G. M. Bolscher, *BioMetals*, 2010, **23**, 569–578, DOI: 10.1007/s10534-010-9306-4.

74 L. Ruiz-Mazón, G. Ramírez-Rico and M. de la Garza, *Explor. Drug Sci.*, 2024, **2**, 734–743, DOI: 10.37349/eds.2024.00072.

75 K. Kosznik-Kwaśnicka, A. Necel and L. Piechowicz, *Front. Cell. Infect. Microbiol.*, 2026, **16**, 1758422, DOI: 10.3389/fcimb.2026.1758422.

76 N. Bruni, M. T. Capucchio, E. Biasibetti, E. Pessione, S. Cirrincione, L. Giraudo, A. Corona and F. Dosio, *Molecules*, 2016, **21**, 752, DOI: 10.3390/molecules21060752.